A Scalable Multi-Probe System for Simultaneous Neuropixel Recordings Across Multiple Cortical Regions in Nonhuman Primates

Emily Sperry

A thesis

submitted in partial fulfillment of the

requirements for the degree of

Master of Science

University of Washington

2026

Committee:

Amy Orsborn

Jeffrey Herron

Program Authorized to Offer Degree:

Bioengineering

University of Washington

Abstract

A Scalable Multi-Probe System for Simultaneous Neuropixel Recordings Across Multiple Cortical Regions in Nonhuman Primates

Emily Sperry

Chair of the Supervisory Committee:

Amy Orsborn

Bioengineering/Electrical Engineering

Understanding how distributed motor circuits coordinate complex behavior requires recording technologies capable of simultaneously capturing large-scale, depth-resolved neural activity across multiple cortical areas in clinically relevant animal models. Existing systems for nonhuman primate (NHP) electrophysiology fail to meet this need: single-probe designs preclude simultaneous multi-area sampling, multi-probe designs suffer from mechanical instability at larger probe counts, and no existing platform integrates optical stimulation as a primary design constraint. This thesis addresses these gaps through two aims: the development and validation of scalable multi-probe Neuropixels fixtures for rhesus macaques, and the development of supporting software and phantom-based characterization tools for atlas-guided probe targeting.

Two complementary fixture designs were developed to span the trade-off between spatial flexibility and simultaneous channel count. The three-probe linear fixture supports session-by-session repositionability across the rostrocaudal extent of motor cortex, consolidating three

Neuropixels probes into a narrow linear body that preserves the approximately 10 mm accessible cortical footprint of the single-probe predecessor. The six-probe fixture maximizes simultaneously recorded channel count and integrates co-registered optical fibers for optogenetic stimulation, enabling dense, multimodal sampling of a fixed cortical footprint. Both fixtures share a single shared drive mechanism for simultaneous probe advancement, incorporate structural isolation between probe mounts to prevent electromagnetic cross-talk, and include a locking mechanism for probe retention during recording. Electrical characterization confirmed that inter-probe coherence in both fixtures was limited to environmental 60 Hz line noise, with no stimulus-locked cross-talk detected across the full neural recording frequency range.

Phantom insertion testing using ballistic gelatin established that Neuropixels probe trajectories are highly repeatable under controlled conditions, with single-probe insertions across 15 trials producing tracks of maximum width 0.111 mm and depth 6.3 mm. Multi-probe testing revealed that probe shank curvature is the primary source of inter-probe separation error, producing deviations of up to approximately 1 mm from the 4.8 mm nominal spacing in the three-probe fixture when probes of varying visual straightness are used. Visual pre-screening for probe straightness is identified as a practical and effective mitigation. Brain-geometry phantom testing demonstrated that cortical surface curvature reduces net tip displacement relative to flat-phantom predictions, suggesting that flat-surface measurements represent a conservative upper bound on in vivo trajectory error.

StereoPlan, a Python-based desktop application, was developed to fill the gap in NHP-compatible probe trajectory planning tools. Built around the NIMH Macaque Template v2.0 and the CHARM cytoarchitectonic atlas, it provides interactive 3D probe placement, atlas-labeled

tissue-sequence readout, bend-tolerance cylinder sampling, and a population reach heatmap for target-driven entry point selection.

Together, these contributions establish the hardware, software, and methodological infrastructure required to conduct simultaneous, multimodal, laminar-resolution recordings across distributed motor cortical circuits in a clinically relevant primate model, and provide a foundation for future in vivo validation and extension to additional cortical areas.

Contents

Chapter 1: Introduction

Complex motor and cognitive skills are fundamental to nearly all aspects of human function, from the fine manual dexterity required for tool use to the executive control that enables flexible, goal-directed behavior in dynamic environments. These abilities are not localized to a single brain region; rather, they emerge from the coordinated activity of distributed neural circuits spanning multiple cortical and subcortical areas. For example, skilled reaching and other complex motor behaviors emerge from the coordinated activity of distributed motor cortical circuits [1] — in particular, the dorsal premotor cortex (PMd) and primary motor cortex (M1) — that span multiple areas arranged along the rostrocaudal axis of cortex. PMd is thought to play a key role in movement planning and the selection of actions based on contextual cues, while M1 is more directly involved in movement execution [2]. Because these regions are spatially distinct and interact across large numbers of neurons, understanding their joint dynamics during behavior requires recording methods that can simultaneously capture activity across both areas with high spatial and temporal resolution. Developing the models and methods needed to study these distributed circuits is therefore a prerequisite for progress in understanding motor control.

Models are well established and generally are constrained to mice and nonhuman primates (NHPs), but there is no recording technology that perfectly fits the recording requirements needed for studying distributed circuits. A range of electrode technologies have been applied in models, each with fundamental trade-offs that limit their suitability for capturing widespread, depth-resolved, multi-area dynamics. Electrocorticography arrays offer broad cortical coverage, but sample aggregate population signals from the cortical surface, reflecting input from neurons across the column below each electrode without the spatial resolution needed to distinguish

laminar structure or isolate single-unit activity — both of which are thought to be important for inter-area communication [3]. Utah arrays provide stable, chronically implanted recordings of single units, but are constrained to a small cortical patch with fixed electrode spacing and rigid depth. They do not permit flexible multi-region access, and deploying multiple arrays across cortical areas introduces substantial surgical complexity without enabling the flexible, session-by-session targeting that hypothesis-driven multi-area experiments require. Broad cortical coverage, laminar depth resolution, and flexible session-by-session repositionability are precisely the three properties needed to characterize how motor circuits interact during complex behavior — and no existing recording technology provides all three simultaneously.

Neuropixels probes are an emerging technology that holds promise to address all three needs. A Neuropixels 1.0 probe carries 384 configurable active channels, and in rodents single insertions routinely yield 200–500 well-isolated units spanning the full cortical depth — roughly an order of magnitude improvement over conventional silicon probes [4]. Their slender profile and high channel density make them well-suited for resolving laminar structure, tracking neurons across behavioral epochs, and recording from multiple cortical and subcortical targets in parallel. Deploying multiple Neuropixels probes simultaneously thus offers a path toward the kind of widespread, depth-resolved, multi-area recordings needed to study distributed circuit dynamics during complex behavior.

Within mouse models, a number of fixtures have been designed to accommodate the simultaneous insertion of multiple Neuropixels probes [5], [6]. However, mice are limited as models for studying the kinds of complex motor and cognitive behaviors most relevant to human function. Their cortex is substantially smaller and less differentiated than primate cortex, constraining both the spatial separation of motor areas and the complexity of behaviors they can

learn [7]. NHPs, by contrast, possess a cortex with well-defined homologs of human motor areas, can acquire rich behavioral repertoires comparable in complexity to human motor skills, and have long served as the primary translational model for motor cortex research [8]. Existing NHP recording systems, however, fall short of what is needed. Current designs that accommodate Neuropixels probes in NHPs typically deploy one or a small number of electrodes through a single chamber, restricting access to a limited cortical footprint, forcing recordings from different regions into separate sessions, and precluding simultaneous access to the full set of regions of interest.

An additional limitation of existing systems is the absence of integrated support for multimodal interrogation. Optogenetics — the use of light-sensitive opsins to activate or silence genetically targeted neuron populations with millisecond precision — is a powerful tool for establishing causal relationships between neural activity and behavior, rather than merely observing correlations [9]. Combining optogenetic stimulation with large-scale electrophysiology in the same recording session is therefore critical for moving from descriptive to mechanistic accounts of multi-area motor circuit function. Existing NHP Neuropixels fixtures do not provide integrated optical access, meaning optogenetics must be added on in ways that compromise recording quality or surgical simplicity.

Taken together, these gaps motivate the development of a new multi-probe recording system for NHPs that satisfies four design goals: (1) broad cortical access with flexible probe placement across multiple regions; (2) simultaneous multi-probe recording; (3) session-to-session repositionability, allowing retargeting across recording days; and (4) integrated multimodal capability, with optical stimulation built in rather than added on.

The two aims of this thesis are to address these gaps directly. First, develop and validate new multi-Neuropixels fixtures designed to meet the full set of requirements for a NHP multi-probe recording system. Second, quantify and develop predictive models of Neuropixels probe trajectories, providing the methodological foundation needed to reliably target specific cortical regions and depths across recording sessions. Together, these contributions establish the hardware and methodological infrastructure required to study distributed motor circuit dynamics in a clinically relevant primate model.

1.1 Thesis Overview

Chapter 2 reviews the technical background across six areas relevant to the systems developed here: Neuropixels probe technology, NHP recording chamber infrastructure, brain motion and recording stability, existing multi-probe system designs and their limitations, atlas-based probe targeting tools, and optogenetics in NHPs. Chapter 3 defines the engineering requirements for both fixture designs and for the accompanying software tool, grounded in the failure modes identified in the two preceding hardware generations described at the end of Chapter 2. Chapter 4 describes the hardware implementation of both fixtures, including rejected design iterations, the chamber infrastructure, and the custom assembly tooling developed to make probe installation reliable under vivarium conditions. Chapter 5 presents validation experiments characterizing the mechanical, electrical, and targeting performance of the systems against the Chapter 3 requirements. Chapter 6 describes experiments performed to characterize the tolerance of probes when inserted into phantom brain tissue. Chapter 7 describes StereoPlan, the Python-based probe trajectory planning tool developed to support both fixtures. Chapter 8 discusses the key findings, compares the designs to prior work, and outlines recommendations for future development.

Chapter 2: Background

This chapter develops the technical and scientific context needed to understand the design goals of the recording system built in this thesis. It begins with the recording technology at the center of this work — Neuropixels probes — and the physical infrastructure required to deploy them in macaques. It then covers the engineering challenges that arise in that setting: brain motion and recording stability, the demands of multi-probe deployment, and the integration of optogenetics for causal inference. Finally, it describes the atlas-based targeting tools available for NHP experiments and the two prior generations of hardware developed in this lab, whose successes and failure modes directly motivated the systems described in subsequent chapters.

2.1 Neuropixels Probe Technology

The central bottleneck in systems neuroscience has long been that the number of neurons that can be recorded simultaneously grows far more slowly than the number known to participate in the behaviors under study [10]. Neuropixels probes represent the most significant recent advance against this bottleneck, and are the recording technology of choice for this work because they uniquely combine high channel count, laminar depth resolution, and a slender profile compatible with NHP chamber constraints. The Neuropixels 1.0 probe integrates 960 low-impedance recording sites on a 70 × 10 μm shank at 20 μm vertical spacing, with a user-configurable bank of 384 simultaneously active channels. On-shank CMOS circuitry digitizes signals before transmission, achieving input-referred noise of 5–7 μV RMS in the action potential band (300–10,000 Hz) [4]. In rodents, single insertions routinely yield 200+ well-isolated units spanning the full cortical depth, roughly an order of magnitude improvement over conventional silicon probes

[11] — and the dense vertical sampling enables laminar resolution of population activity that ECoG and Utah arrays cannot provide.

Extracting single units from high-channel-count recordings requires spike sorting algorithms designed for this data regime. Kilosort [12] and MountainSort [13] exploit the spatial spread of individual unit waveforms across neighboring sites to disambiguate overlapping spikes. Sorting quality is sensitive to probe stability: drift of even a few micrometers shifts the waveform profile of each unit across channels, creating apparent template changes that split or merge units. Drift correction modules have been integrated into Kilosort and related tools [14], but minimizing physical probe motion through mechanical design remains important for the highest-quality single-unit isolation.

2.2 NHP Recording Chambers & Cortical Access

Deploying Neuropixels probes in macaques requires a physical infrastructure that differs substantially from rodent preparations. The standard infrastructure for NHP electrophysiology is the recording chamber — typically a titanium or PEEK cylinder implanted over a craniotomy and fixed to the skull with bone cement and titanium screws — supporting a removable grid through which electrodes or probes are advanced [15]. The grid defines the coordinate system used to target cortical locations across sessions, and also allows for gentle pressure to be applied to the brain surface to stabilize it.

A complication specific to macaques is the native dura mater, which is substantially tougher than rodent dura, with a thickness of 0.3–0.5 mm and tensile properties that deflect or damage fine recording electrodes on insertion [16]. Standard approaches include mechanical thinning of the dura before each session or complete durotomy with dural regrowth between sessions, but both

generate cumulative tissue damage: thinning produces inconsistent results across sessions, and repeated durotomies generate scar tissue that progressively degrades recording quality and limits the usable chamber lifetime [17].

Artificial dura replacements, typically fabricated from polydimethylsiloxane (PDMS) or similar optically transparent biocompatible elastomers, address these limitations by substituting a compliant, stable material for the native dura after a single durotomy [18]. The artificial dura presents negligible resistance to electrode insertion, permits repeated access without additional surgery, and — owing to optical transparency — supports simultaneous imaging and optical fiber delivery. Long-term biocompatibility of PDMS artificial dura has been demonstrated in NHPs, with stable cortical access maintained over months to years and without the progressive tissue ingrowth that degrades access through repeatedly incised native dura [18].

2.3 Brain Motion and Recording Stability

Even with a well-designed chamber and artificial dura, achieving stable single-unit recordings in awake macaques is complicated by brain pulsatility. Cardiac-driven cyclic tissue deformation occurs at 1–3 Hz in awake macaques, with cortical surface excursions of 20–100 μm depending on proximity to major vessels [19]; respiratory motion adds a slower component at 0.2–0.5 Hz with similar or larger amplitude [20]. For a probe held fixed relative to the skull, this tissue motion produces relative displacement between the probe and the recorded neurons, manifesting as waveform drift and, in severe cases, complete loss of unit isolation.

Mechanical stabilization of the cortical surface is the primary mitigation strategy. A flat or conforming grid placed in contact with the cortical surface through the artificial dura applies gentle distributed pressure that damps pulsatile excursion without causing ischemic damage to

superficial vascular layers [21]. Grid geometry must balance adequate contact pressure for motion suppression against minimal vascular interference, and in systems where the grid doubles as the probe positioning matrix, aperture spacing and geometry must additionally accommodate the insertion angles required to reach target structures.

Software drift correction provides a complementary approach. Kilosort and related algorithms estimate probe drift from the slowly shifting spatial distribution of recorded unit templates and compensate during template matching [12]. This approach handles slow, smooth drift well but is less effective for rapid pulsatile motion, and requires sufficient unit density across the probe to estimate the drift profile reliably. Mechanical stabilization and software correction are most effective in combination: the former suppresses high-frequency pulsatile motion, the latter handles residual slow drift. Both of these mitigation strategies place direct demands on fixture design: the mechanical contact geometry of the grid must be compatible with surface stabilization, and the fixture must hold probes rigidly enough that its own compliance does not add a noise source on top of the biological motion it is designed to suppress.

2.4 Multi-Probe System Design

The three recording needs established in Chapter 1 — broad cortical coverage, laminar depth resolution, and session-to-session repositionability — cannot be met by a single probe. Inter-areal communication, the exchange of signals between cortical regions during behavior, cannot be adequately studied from within any single area. Sequential recordings across separate sessions provide useful data, but cannot capture the moment-to-moment covariation between populations that reflects the dynamic coordination of distributed circuits [22]. Achieving this requires simultaneously deploying multiple high-density probes across cortical areas.

Existing multi-probe systems reveal a consistent gap in the field. The multi-probe manipulation rig developed at Janelia Research Campus uses motorized, multi-axis drives to achieve precise and independently controllable probe positioning [6]. While this confers accurate acute targeting, the large mechanical footprint of the drive assemblies limits compatibility with many recording configurations, and the design was developed for rodent preparations, making it poorly suited to the spatial constraints of NHP chambers. A different approach uses a lightweight, head-mounted fixture for chronic Neuropixels recordings in freely moving rats [5]. This achieves stable recordings over months — a considerable advantage for tracking the same neural population longitudinally — but at the cost of spatial flexibility: probe positions are fixed at implantation, precluding the session-by-session repositioning needed for systematic cortical mapping.

The translation of high-density silicon probe recording to NHPs was advanced by a chamber system capable of large-scale neural recording in macaques [21] , which established that the single-session unit yields achievable with Neuropixels in rodents could be approached in NHPs, and demonstrated engineering principles — including controlled insertion speed and mechanical isolation from external vibration — that have informed subsequent implementations. Nevertheless, the targeting range of this system is restricted to approximately 5 mm within the chamber, limiting access to a narrow cortical footprint and making simultaneous sampling of widely separated areas difficult.

Across these systems, a consistent pattern emerges: acute systems trade coverage for precision; chronic systems trade flexibility for stability; and in both cases multimodal integration is largely an afterthought. No existing design simultaneously provides flexible access to a broad cortical area, session-to-session repositionability, and physical accommodation of both multiple probes

and optical hardware within the same chamber. The fixture architecture developed in this thesis treats these demands as primary design constraints from the outset.

2.5 Optogenetics in NHPs

While multi-probe electrophysiology reveals the correlational structure of distributed circuit activity, establishing causal relationships between neural populations and behavior requires experimental manipulation. Optogenetics, which uses virally delivered light-sensitive opsins to make defined neuronal populations responsive to optical stimulation, provides a means of doing this with cell-type specificity and millisecond temporal precision that electrical stimulation cannot match [23]. In macaques, AAV-mediated delivery of channelrhodopsin-2 (ChR2) or inhibitory opsins under promoters such as CaMKIIα for excitatory neurons or mDlx for GABAergic interneurons has been used to dissect the contributions of defined populations to a range of behaviors, and the approach has been validated in motor, visual, and prefrontal cortex [24], [25].

Incorporating optical stimulation into a multi-probe recording system requires each optical fiber to be positioned as close as possible to the recording probes, with the fiber tip placed within the transduced volume to achieve stimulation intensities above the activation threshold at the cortical surface. This adds spatial and mechanical demands to an already constrained fixture design: fiber ferrule connectors are substantially larger than the fibers themselves and must be accommodated at the top of each mount, and the fibers must be routable away from the recording field without coupling mechanically to adjacent probes. The effective stimulation radius for blue-light ChR2 activation at the cortical surface is approximately 1 mm, given the scattering and absorption

properties of cortical tissue at 470 nm [26], which means that fiber placement accuracy is directly consequential for experimental outcomes.

2.6 Neuropixels Probe Deflection and Trajectory Uncertainty

A largely uncharacterized source of targeting error in Neuropixels experiments is mechanical deflection of the probe shank during insertion. Neuropixels shanks are long, slender structures — the 1.0 shank extends 10 mm at a cross-section of just 70 × 20 µm — and are therefore subject to bending forces when they encounter resistance during insertion into neural tissue. These forces arise from a combination of factors: the mechanical resistance of the tissue itself, which varies with local density and vasculature; the angle of entry relative to the cortical surface, which determines the lateral load component on the shank tip; and the unsupported length of the probe between the grid aperture and the tissue surface, which acts as a cantilevered beam and amplifies small lateral forces into tip displacement. Any combination of these factors can cause the probe to follow a curved rather than straight trajectory through the brain, meaning the shank tip — and therefore the recording sites — may end up displaced from the intended target by an amount that is difficult to predict from insertion coordinates alone.

This matters particularly in NHP experiments, where histological verification of probe placement cannot be performed routinely and targeting relies primarily on atlas registration and surface landmarks. In rodents, the short distances involved and the high frequency of terminal experiments mean that trajectory errors are often caught post-hoc or tolerated within the uncertainty of the atlas registration. In NHPs, by contrast, the greater insertion depths required to reach target structures, the inability to confirm placement histologically within an ongoing experiment, and the clinical relevance of precise area targeting all make trajectory uncertainty a

more consequential problem. Despite this, probe deflection in NHP tissue has not been systematically quantified, and existing trajectory planning tools — including those described in the following section — assume straight-line probe paths from entry point to target.

Characterizing this deflection empirically, and incorporating measured deflection tolerances into the targeting workflow, is therefore a necessary step toward reliable multi-probe NHP recording. This is the focus of Aim 2 of this thesis: quantifying how much Neuropixels probes deflect under realistic NHP insertion conditions, identifying the factors that predict deflection magnitude, and integrating that characterization into the StereoPlan targeting tool so that planned trajectories account for expected tip displacement rather than assuming idealized straight-line insertion.

2.7 Atlas-Based Probe Targeting

Accurate targeting across sessions requires aligning experimental coordinates to a neuroanatomical reference. This is more challenging in NHPs than in rodents: histological verification of probe placement cannot be performed routinely, so target localization must generally be estimated from surface landmarks and MRI-based registration, placing a higher burden on pre-surgical planning and coordinate bookkeeping.

Probe trajectory planning tools have been developed primarily for the rodent community. Pinpoint provides an interactive 3D interface in which virtual probes are inserted into a registered brain volume and their trajectories through annotated atlas regions visualized in real time [27]. BrainGlobe provides atlas registration pipelines, region-of-interest querying, and integration with spike sorting workflows [28]. These tools have been extended to several non-rodent species including macaques, but do not natively account for the constraints imposed by a physical recording chamber grid — specifically, that probes must enter through fixed grid

apertures at angles constrained by the chamber geometry — which is the dominant targeting constraint in NHP multi-probe experiments. StereoPlan, described in Chapter 7, was developed to fill this gap directly.

2.8 Prior Work

The system developed in this thesis builds directly on two preceding generations of NHP Neuropixels hardware developed in lab, each of which established capabilities and identified the failure modes that shaped the designs in subsequent chapters.

The first system was a single-probe acute recording platform designed to maximize spatial coverage across the cortical surface within a single chamber. The probe was mounted on a Narishige hydraulic microdrive and introduced through a custom grid insert that registered to the chamber coordinate system, enabling systematic targeting of locations distributed across approximately 1 cm² of cortical surface through movement in x, y, and z directions. The narrow mechanical footprint of the single-drive assembly left sufficient clearance to route optical fibers to selected locations alongside the probe shank, enabling multimodal electrophysiology and optogenetic stimulation within the same session. This design achieved probe drift of less than 20 µm across sessions and maintained stable single-unit recordings over more than 30 consecutive recording days, validating the artificial dura and grid system as a reliable foundation for longitudinal NHP Neuropixels work. However, its inherently

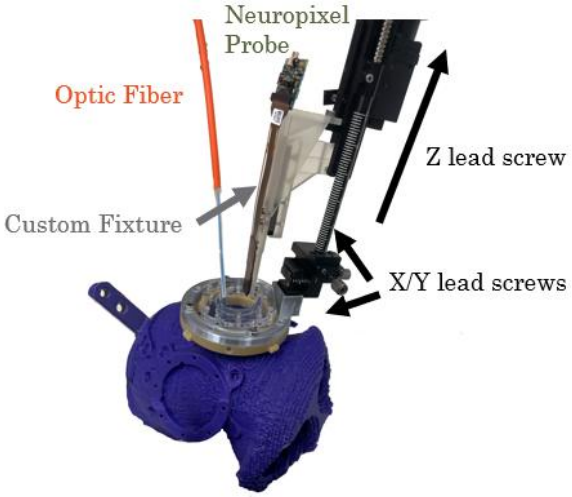

Figure 1 Setup of first generation used in the Orsborn Lab. The design deploys a single Neuropixel probe advanced on a single Narishige Drive. An optic fiber is shown inserted relative to the probe

serial nature — one probe per session — precluded the simultaneous multi-area recordings necessary to study inter-areal dynamics.

The second system extended this platform to two simultaneously deployed probes, motivated by the need to capture correlated activity between cortical areas within single sessions. Two Neuropixels probes were mounted on independent Narishige hydraulic drives, each capable of independent x–y translation, allowing flexible positioning of the two probes relative to one another without constraining them to fixed relative locations. The assembly was designed for rapid setup in the vivarium and reused the grid insert established in the first-generation system, preserving compatibility with the existing targeting workflow. In practice, however, the combined mass of two Narishige drives produced a mechanically unstable assembly: the drives interfered with each other's range of motion, and the weight of the combined structure introduced vibration and positional uncertainty that degraded recording stability. The spatial flexibility of the two-probe system was therefore substantially limited relative to its design intent, and the mechanical constraints made extension to three or more probes with this architecture impractical.

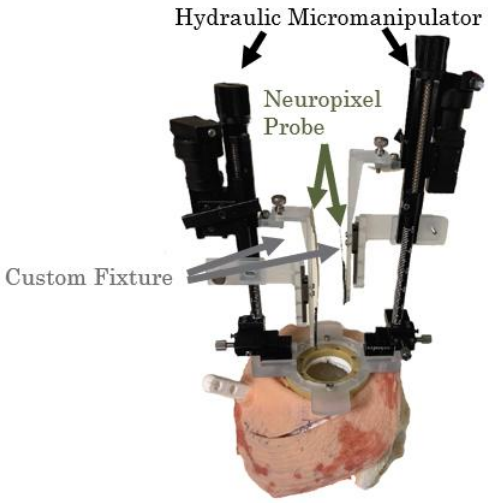

Figure 2 Second generation design used in the Orsborn lab. The design deploys Neuropixels simultaneously on independent Narishige hydraulic drives

These two generations together define the starting point for this thesis. The single-probe platform demonstrated that stable, high-yield NHP Neuropixels recordings are achievable with this chamber infrastructure over long timescales, and confirmed the feasibility of co-deploying optical fibers within the same recording footprint. The two-probe system demonstrated that

independent drive mechanisms are necessary for flexible multi-area targeting, but that drive mass and mechanical coupling are the primary failure modes at larger probe counts — a finding that directly motivated the modular, low-mass fixture architecture described in Chapter 3.

Chapter 3: System Design and Requirements

The failure modes identified in Section 2.8 — mechanical instability from drive mass, insufficient probe isolation, and the absence of integrated optical access — defined the design space for the next generation of hardware. Two complementary fixture designs were developed in response, each optimized for a distinct experimental use case and together spanning the trade-off between spatial flexibility and simultaneous channel count. The first is a three-probe linear fixture that prioritizes session-to-session repositionability, enabling systematic sampling of different cortical areas across days. The second is a six-probe fixture with co-registered optical fibers that prioritizes maximizing simultaneously recorded channel count and enabling optogenetic integration at a fixed cortical footprint. The two designs are intended to be complementary: the three-probe fixture addresses experiments that require flexible targeting across the rostrocaudal extent of motor cortex, while the six-probe fixture addresses experiments that require dense, multimodal sampling of a well-characterized set of cortical locations. Both designs share a set of overarching constraints imposed by the NHP recording context, described in Section 3.1, before diverging in their design-specific requirements.

3.1 Shared Requirements

Both fixture designs are subject to the same physical and operational constraints imposed by the NHP recording environment. The functional lower portion of each fixture must fit within a 20 mm diameter recording chamber, which in practice presents an even more restricted aperture once standard chamber inserts such as guide grids and adapters are accounted for. Total system weight must be minimized to reduce burden on the animal, imposing strict limits on the mass of all structural and mechanical components. Both systems must also be compatible with the

standard sterile field and procedural constraints of NHP recording sessions, including the requirement that all assembly steps performable only under personal protective equipment be minimized. Components requiring fine manipulation or bench-level tolerances can be assembled prior to deployment and left intact for the operational lifetime of the fixture, reducing procedural complexity during recording sessions.

The primary functional requirement shared by both designs is the ability to advance multiple Neuropixels probes simultaneously from a single shared drive mechanism. The two-probe predecessor required independent manual advancement of each probe, making it difficult to ensure consistent insertion depth across probes given variability in cortical surface geometry and dural resistance across the chamber. A single shared drive eliminates this ambiguity by coupling probe advancement mechanically, ensuring that all probes within a given fixture reach equivalent depths during insertion.

Both fixtures must hold probes in a fixed geometric relationship to one another throughout insertion, maintaining perpendicular entry relative to the cortical surface. Perpendicular insertion minimizes lateral tissue displacement and the associated risk of probe damage during advancement, and simplifies the geometric assumptions required for atlas-based estimation of probe location. Any deviation from perpendicularity introduces a systematic offset between the planned and actual probe trajectory, compounding the trajectory uncertainty described in Section 2.6 and complicating post-hoc localization.

Each probe must be secured to its mounting interface in a manner that prevents inadvertent displacement during recording. In the two-probe predecessor, insufficient probe retention posed a risk of probes shifting during a session. Both new designs therefore incorporate a locking

mechanism that secures each probe carrier once positioned, engageable without excessive force or fine motor precision under sterile conditions.

A key mechanical lesson from the two-probe design was the importance of physically isolating adjacent probes and their associated headstages from one another. When probe cables were free to move and approach neighboring headstages, electromagnetic coupling introduced noise into the recording. Both new designs therefore incorporate structural material between each probe mount and its neighbors, constraining cable geometry and ensuring that no two headstages can come into proximity during a session. Cable routing for each probe is directed away from neighboring headstages and secured against movement, minimizing the potential for inter-probe electromagnetic interference.

3.2 Three-Probe Fixture Requirements

The three-probe fixture is the flexible complement to the six-probe design. Its defining requirement is session-to-session repositionability: the fixture must be translatable within the chamber across recording days, allowing the experimenter to access different cortical areas and approach trajectories systematically. This makes it well suited to experiments targeting the rostrocaudal arrangement of motor cortical areas relevant to reaching — in particular PMd and M1 — where the optimal probe placement may differ depending on the behavioral epoch or hypothesis under study.

To accommodate variability in cortical targets across experiments and animals, the fixture must also support modularity in probe configuration. It must be possible to mount either two or three probes depending on the targets of interest, and to vary the spacing between probes to match the geometry of the relevant cortical regions. This modularity necessarily constrains the maximum

number of probes that can be accommodated within the chamber aperture, making the three-probe fixture the lower channel-count of the two designs. The gain in spatial flexibility is the intended trade-off.

3.3 Six-Probe Fixture Requirements

The six-probe fixture is the high-yield, multimodal complement to the three-probe design. It is designed for a fixed insertion point used consistently across sessions: the fixture occupies the full chamber aperture and cannot be repositioned, so the precise chamber coordinates of each probe are determined at assembly. The fixture must be lowered and raised from the exact same position on every recording day to ensure reproducible targeting, and any error in chamber-level placement cannot be corrected without removing and repositioning the entire assembly. This demands a higher standard of precision at chamber implantation than the three-probe design, but in exchange it enables the fixture to maximize the number of simultaneously recorded channels — in principle yielding up to 6 × 384 simultaneously active channels — and to incorporate a fixed optical fiber geometry with a known, stable spatial relationship to the probe array.

It is worth noting that while channel count scales linearly with probe number, the number of well-isolated single units does not scale at the same rate, as probes in close proximity may sample overlapping neural populations or compete for access to the same cortical tissue volume. Probe spacing within the six-probe fixture must therefore balance the goal of maximizing coverage against the risk of redundant sampling.

The six-probe fixture incorporates optical fibers co-registered with the probe array, enabling light delivery to targeted cortical regions for optogenetic stimulation. The inclusion of optical fibers in this fixture — rather than the three-probe design — reflects a practical constraint of the

repositionable architecture: because the three-probe fixture is translated across the chamber between sessions, a fixed fiber geometry would bear no stable spatial relationship to cortical targets across recording days and would therefore be of limited experimental utility. In the six-probe fixture, where insertion coordinates are held constant across sessions, a fixed fiber geometry can be reliably related to a known set of anatomical targets, and optical stimulation can be directed to the same cortical locations on every recording day. Each fiber tip must be positioned within approximately 1 mm of the intended stimulation site, consistent with the effective stimulation radius for blue-light ChR2 activation described in Section 2.5, making the spatial relationship between fiber mounts and probe shanks a primary design constraint at assembly.

Chapter 4: Hardware Implementation

This chapter describes the physical implementation of the two fixture designs whose requirements were established in Chapter 3. Section 4.1 documents the iterative development process and the approaches that were pursued and rejected before the final configurations were established. Sections 4.2 and 4.3 describe the three-probe and six-probe fixtures respectively. Section 4.4 covers the chamber infrastructure common to both, including the artificial dura, chamber inserts, and the adapter system through which the fixtures interface with the skull implant.

4.1 Design Iterations and Rejected Approaches

The current fixture designs are the result of several iterative development cycles. A number of design approaches were pursued, built, and rejected before the final configurations were established. This section documents those rejected designs and the specific requirements they failed to meet, as a record of the engineering constraints that ultimately shaped the chosen solutions.

All fixtures share a common mechanical backbone inherited from the single-probe system: a Narishige hydraulic microdrive that attaches to the recording chamber through a chamber adapter & drive holder, a fixture body that holds the probes, and a carriage adapter that couples a miniature ball-bearing linear rail and carriage (McMaster-Carr Product 8381K29) to the drive. This arrangement preserves compatibility with the existing drive system and allows the user to exploit both the coarse and fine adjustment of the Narishige drive, as well as the x/y movement. Iterations on each fixture therefore focused on the geometry of the fixture body and the form of the carriage adapter, rather than on the drive or chamber mounting.

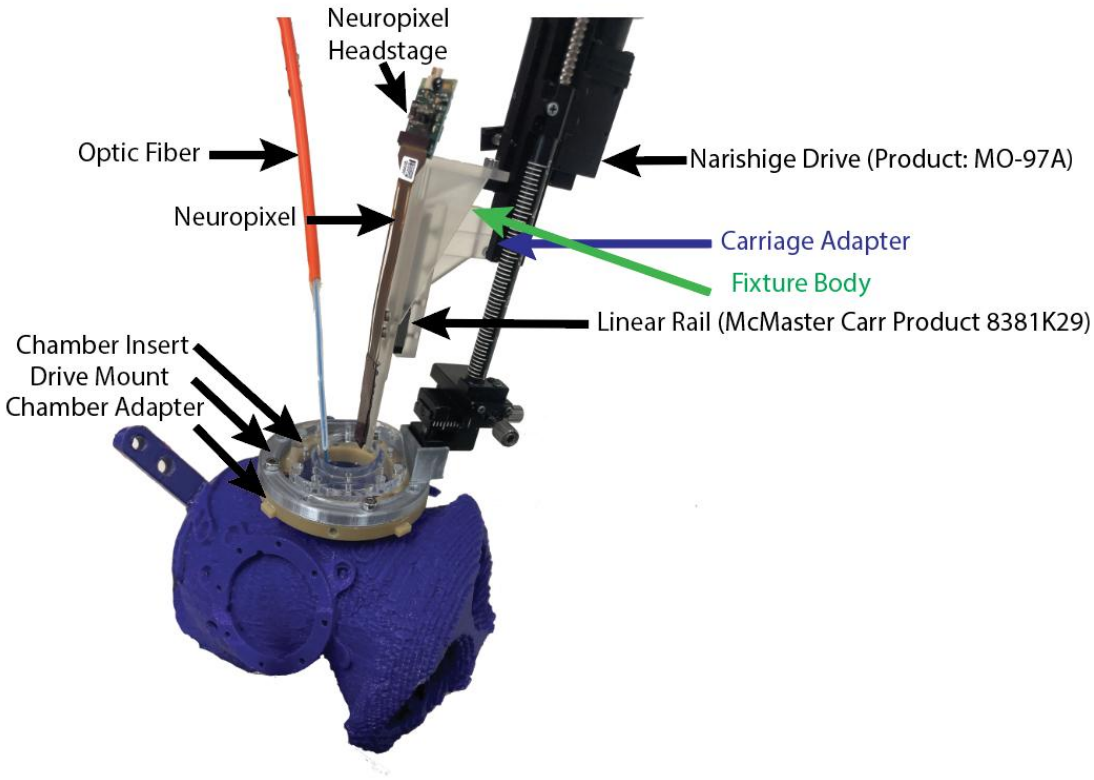

Figure 3 Diagram of components that are part of common mechanical background. Colored labels correspond to features most commonly modified between designs.

4.1.1 Three-probe fixture iterations

The three-probe fixture required relatively few iterations owing to its more relaxed spatial constraints. An initial concept placed probes on individual separate parts that were assembled together, but this was rejected because it increased the overall width of the assembly beyond the chamber aperture and introduced additional failure modes at each inter-part interface.

The approach that carried forward consolidated the three probe mounts into two physical parts: a primary body holding two probes back-to-back, and a secondary piece that screws onto it to hold the third. This two-part split provides inherent modularity — experiments requiring only two

probes can be conducted without attaching the third-probe piece — and was retained through all subsequent versions.

4.1.2 Six-probe fixture iterations

The six-probe fixture required more extensive iteration owing to the tighter constraints imposed by the full chamber aperture. Three major approaches were pursued and rejected before the final design was established.

Figure 4 Hexagonal design first explored for six probe fixture.

The earliest concept arranged all six probes in a hexagonal pattern with each probe facing outward toward the chamber wall. This design failed the inner diameter constraint: by not accounting for the aperture reduction imposed by the chamber insert, the probe tips were placed too close to the chamber walls, creating an unacceptable risk of probe breakage on insertion. The hexagonal geometry was abandoned entirely as a result.

A second approach tested whether probe dovetails could be loaded from the top into slots in the fixture body rather than slid in laterally. In practice, this produced unacceptably thin wall sections that were deemed too fragile for repeated use. Because this version was also a single solid piece at the base, there was no space to mount headstages or to route cables away from one another, violating the cable isolation requirement established in Section 3.1.

A near-final design divided the fixture into two halves that mated together, each holding three probes in a roughly triangular arrangement, with holes through the center of each half intended to route optical fibers. This design resolved the cable routing and aperture problems but introduced

a new failure mode: probes were retained by friction alone, with no positive locking mechanism. Because the fixture was intended to be machined from metal — which provides precise fits with little inherent friction — probes could slip during use, particularly after repeated insertion cycles. The absence of a reliable locking mechanism was the disqualifying failure and directly motivated the set-screw interface used in the final design.

4.2 Three-Probe Linear Fixture

The three-probe fixture is a linear, session-repositionable assembly designed to sample simultaneously from motor cortical areas arranged along the rostrocaudal axis, principally PMd and M1. It implements the modularity and repositionability requirements of Section 3.2 through a two-part probe-holding body and a shared single drive mechanism.

The primary body holds two probes back-to-back and connects directly to the Narishige drive via the original single-probe carriage adapter. The secondary piece screws onto the primary body to hold the third probe and can be omitted entirely for two-probe sessions, reducing assembly time and the number of probes at risk. Each part secures its probes via a compliant clamping mechanism: a gap machined into the fixture body is bridged by a threaded screw, and tightening the screw draws the gap closed and applies compressive force on the probe dovetail. A single screw per part is

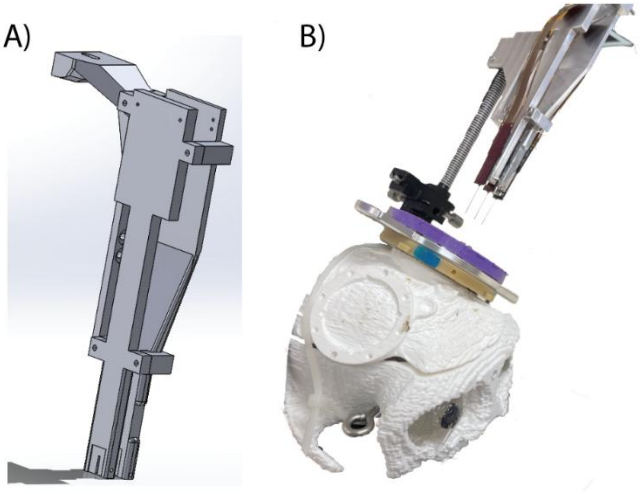

Figure 5 Three-probe linear fixture design and physical implementation. (A) CAD model in SolidWorks showing the two-part probe-holding body and clamping mechanism. (B) Fully assembled fixture mounted on a model chamber.

sufficient — on the two-probe primary body, one screw simultaneously secures both probes. Session-to-session repositionability is achieved by translating the drive in XY through the chamber adapter, allowing the fixture to target different cortical locations across recording days without removing or modifying the fixture itself.

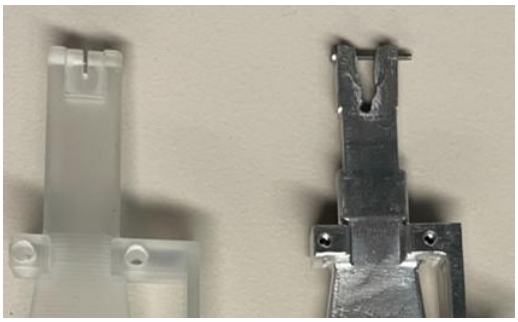

Figure 6 Clamping mechanism before and after post-machining modification. Aluminum version with gap deepened by post-machining to restore clamping compliance and reliable probe retention is shown on the right.

Early prototypes were fabricated in ABS-like resin (WaterShed XC 11122) to enable rapid iteration. The final design was CNC machined from aluminum 6061-T6 by ProtoLabs. The transition to metal revealed a material-dependent behavior in the clamping mechanism: the greater rigidity of aluminum relative to resin meant the machined gap did not close sufficiently under screw tightening to grip the probe dovetail reliably. This was resolved by post-machining the gap deeper with a rotary tool, increasing the compliance of the clamping arms enough to restore reliable probe retention. This finding informed the gap geometry specified for any future remachining of this part. Nominal probe spacing is 4.8 mm center-to-center.

4.3 Six-Probe Fixture

The six-probe fixture is a fixed-array, full-aperture assembly designed to maximize simultaneously recorded channel count and to support integrated optogenetic stimulation from a

single chamber, implementing the requirements of Section 3.3. Because it occupies the full chamber aperture, probe positions are determined at assembly and held constant across sessions, placing a higher requirement on surgical precision at chamber implantation.

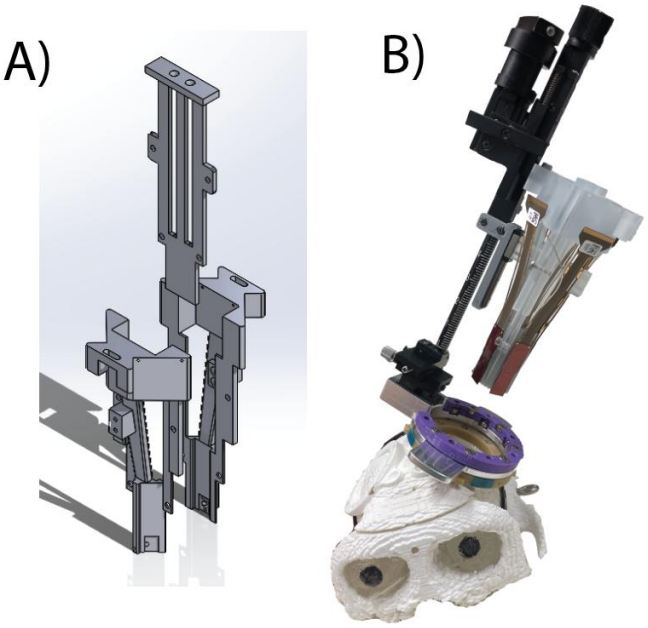

Figure 7 Six-probe fixture design and physical implementation. (A) CAD model in SolidWorks showing the exploded version of the fixture. (B) Fully assembled fixture mounted on a model chamber.

The fixture body is split into two halves, each holding three probes in a roughly triangular arrangement: two probes in each half face outward toward the chamber wall, and one faces the mating surface of the opposite half. Each probe is secured via set screws tightening through holes that face into the dovetail slots, clamping the probe against the fixture body and eliminating the friction-fit failure mode identified during iteration.

Because the six-probe assembly occupies the full chamber aperture, there is no clearance around the outside of the fixture through which optical fibers could be passed independently. A dedicated fiber-routing piece is therefore sandwiched between the two halves, routing optical fibers for optogenetic stimulation to positions co-registered with the probe array without encroaching on the structural walls of the probe-holding bodies. This is in contrast to the

three-probe design, which leaves sufficient open space within the chamber that fibers can be routed alongside the fixture without dedicated hardware. Fiber tip placement is constrained to within approximately 1 mm of the target stimulation site, consistent with the effective ChR2 stimulation radius discussed in Section 2.5.

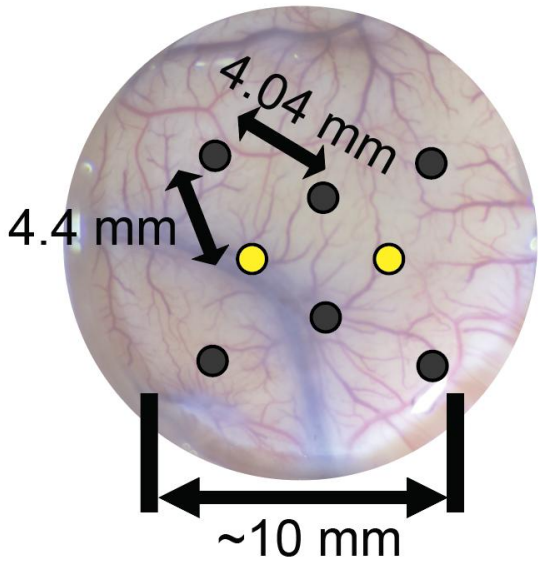

Figure 8 Placement of probes and fibers relative to one another. Probes are shown as grey circles, while fibers are shown as yellow circles.

The six-probe fixture required a shortened carriage adapter relative to the original single-probe design. The original adapter geometry could not position the drive correctly in XYZ space to align with the chamber at the required standoff length. Rather than designing a new chamber adapter — which would have broken reuse compatibility with other fixtures and increased mechanical leverage at the chamber interface — the carriage adapter was shortened instead. This reduces the effective fine-drive travel on the linear rail to approximately 10 mm, compared to approximately 30 mm with the original adapter length, and limits the coarse travel available before the adapter contacts the chamber rim. For the fixed-array use case of the six-probe fixture, where depth adjustments within a session are modest, this travel range is operationally sufficient. It does, however, constrain the system's ability to accommodate larger depth adjustments and represents a known limitation to be addressed in future hardware revisions, most straightforwardly by designing a new chamber adapter that preserves the full travel range while maintaining inter-fixture compatibility.

The fixture is fabricated in ABS-like resin (WaterShed XC 11122).

4.4 Chamber Design and Cortical Access Infrastructure

The recording chamber infrastructure used in this work is a standardized platform [29]. A craniotomy and durotomy approximately 20 mm in diameter is performed over the cortical target, and a titanium implant is screwed to the skull surrounding the opening. An artificial dura, fabricated from PDMS, is placed within the chamber to replace the removed native dura, stabilizing the cortical surface and reducing resistance to probe insertion on each recording day (see Section 2.2 for background on artificial dura). A chamber adapter is then screwed onto the implant, and the drive holder, Narishige drive, and fixture assembly are in turn mounted to the chamber adapter.

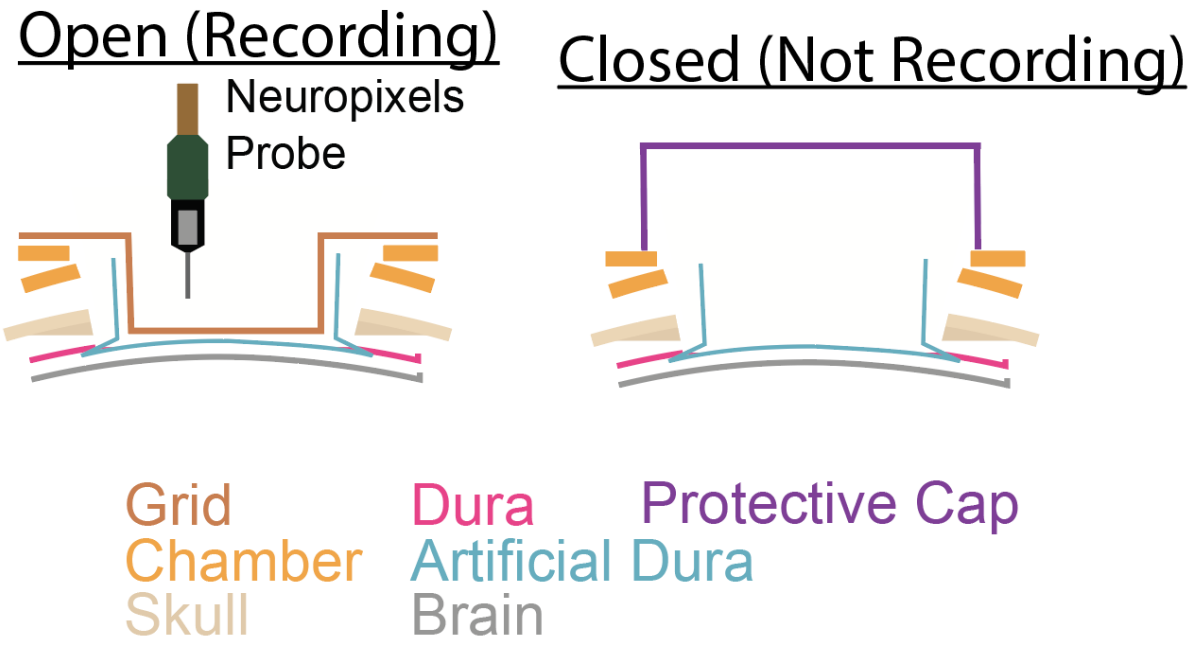

Figure 9 Diagram of chamber interior during and after recording

A chamber insert is screwed into the chamber adapter to constrain probe entry to a defined grid of holes. The original insert used in the laboratory had an inner diameter of 16.8 mm, limiting the

cortical area accessible through it. A new insert was subsequently designed by Tomohiro Ouchi in the lab that increased the inner diameter to 18.3 mm, recovered by thinning the insert walls and relocating the chamber flush ports to the periphery. Both inserts function identically in terms of their role in the recording workflow, but the new insert substantially expands the accessible cortical footprint and is the version used with the multi-probe fixtures described in this thesis.

The two inserts also differ in their rotational flexibility. The original insert could only be mounted in a single orientation relative to the chamber, as there were limited holes in the chamber adapter, so hole-to-brain-region correspondence was estimated by overlaying a numbered hole map onto photographs of the cortical surface and identifying surface landmarks by eye. A new adapter, also designed by Tomohiro Ouchi, includes additional mounting positions that allow the chamber insert to be placed at several different angular orientations, enabling the experimenter to orient the grid to better reach targets near the edge of the accessible area. This flexibility introduces a bookkeeping requirement: the orientation of the insert must be recorded at the start of each session so that hole coordinates can be correctly mapped both to surface landmarks and to the StereoPlan targeting predictions described in Chapter 7.

4.5 Assembly Aids and Custom Tooling

Assembling multi-probe fixtures with Neuropixels probes—which are fragile, expensive, and difficult to handle under personal protective equipment—imposes practical constraints on the assembly process that are distinct from those governing the recording hardware itself. A set of custom jigs and fixtures was designed specifically to make probe installation reliable and repeatable without requiring excessive manual dexterity or fine motor precision.

4.5.1 Three-Probe Assembly Aids

Four assembly jigs were designed for the three-probe fixture. All were printed in-lab on a desktop 3D printer in PLA filament. The assembly sequence proceeds through the jigs in order, with each one addressing a specific handling risk.

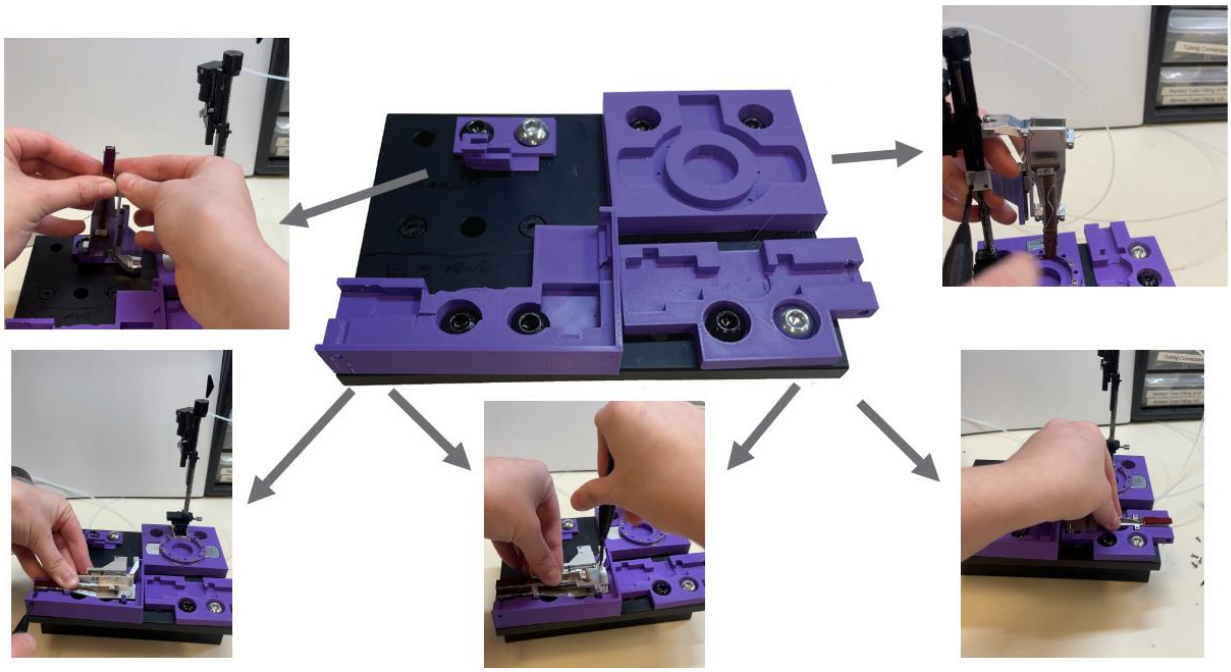

Figure 10 Assembly jigs with example usage.

The first jig holds the two-probe half upright and freestanding while probes are loaded onto it. Because this half is already attached to the carriage adapter at this stage, the jig is sized to accommodate the full carriage adapter footprint. The practical benefit is that once the first probe is slid onto the fixture, the jig holds the assembly steady while the experimenter retrieves the second probe from its storage box, eliminating the need to hold the partially loaded fixture in one hand—a significant risk reduction given that a probe already on the fixture is vulnerable to being knocked or bumped during that interval.

Once both probes are on the two-probe half, the assembly is transferred to the second jig, which serves two functions. First, it holds the half securely in a fixed orientation. Second, and more critically, it provides a precisely positioned guide hole through which a screwdriver can be inserted to tighten the clamping screw. Without this guide, the screwdriver must be brought in freehand very close to the probe shanks; historically this resulted in the screwdriver slipping and contacting a probe on roughly half of assembly attempts or more. With the jig in place, the screwdriver path is constrained and the risk of contact is substantially reduced. After tightening, the two-probe half can be lifted out of the jig, headstages attached to both Neuropixels and connected to the fixture body, and the half set back into the jig temporarily.

The third jig performs the same function for the single-probe half. Once the third probe is slid onto that half and set into the jig, a guide hole allows the clamping screw to be tightened safely. The headstage for this probe is then attached. The single-probe half is subsequently placed onto the two-probe half—which is still seated in the second jig—and the two halves are screwed together with both assemblies stabilized.

The fourth jig holds the Narishige drive and drive holder during the final step of assembly. The drive is first screwed into the drive holder, and the drive holder is then secured into the jig. The fully assembled probe fixture is attached to the drive while the drive holder is fixed in the jig, so that the connection can be made without any free-hand manipulation of the drive near the probes. Once attached, the drive holder is unscrewed from the jig and the complete assembly is ready for use.

4.5.2 Storage Aid

One container with a removable lid was designed to store the completed assembly between uses. Like the fourth jig from the assembly aids, it accepts the drive holder via a screw interface. The interior is fully open below the drive holder seat, and a ledge at the base accepts a removable cup that can be filled with ethanol or another cleaning solution. The drive can be lowered until the probe tips are submerged, allowing sterilization in place without disassembly. Threaded holes in the sides of the aid accept a lid that fully encloses the fixture when not in use, protecting the probes from accidental contact during storage. This means the fixture does not need to be disassembled between recording sessions—only when a probe breaks and must be replaced.

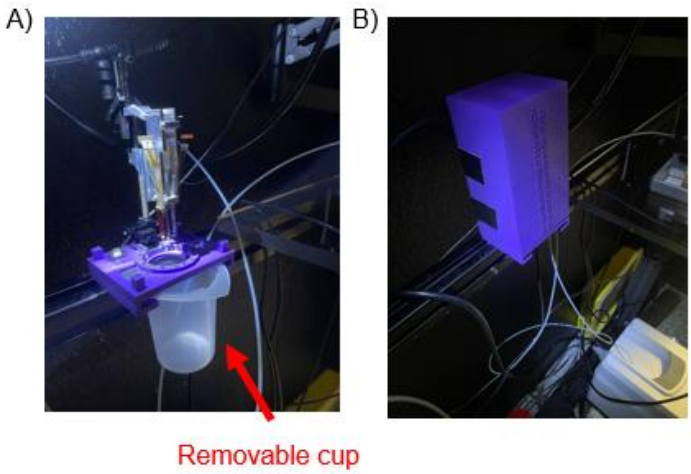

Figure 11 Storage aid attached to a bar in recording booth. (A) Storage with three probe assembly placed inside, and removable cup loaded. (B) Storage with lid securely placed.

Chapter 5: Hardware Verification

This chapter presents verification experiments conducted to characterize the mechanical, electrical, and usability performance of the fixture systems. Testing proceeds from dry fit testing through bench electrical characterization to assembly usability assessment.

5.1 Dry Fit Testing

Dry fit testing was performed to establish the accessible cortical footprint of the three-probe fixture within the recording chamber. This testing was not necessary for the six-probe fixture, which is designed to occupy the full chamber aperture and can only be seated in a single orientation; its probe positions are therefore determined at assembly rather than by intraoperative XY translation.

Testing was conducted by loading the fixture with dummy Neuropixels probes and traversing the extremes of XY travel available through the chamber adapter, verifying at each extreme that no probe contacted the chamber walls. By sampling the boundary of reachable positions in this way, a circular accessible region was defined whose interior represents the full set of cortical locations targetable without probe breakage risk. The three-probe fixture was found to access a region approximately 10 mm in diameter, comparable to the accessible footprint of the single-probe predecessor. This parity is notable given that the fixture carries three probes simultaneously; the consolidation of probe mounts into a narrow linear body, rather than a laterally distributed arrangement, preserved the effective working radius of the drive system.

However, access across the full reachable region is not uniform with respect to probe count. At positions near the boundary of the accessible circle, the presence of a third probe introduces a risk of wall contact that is absent when only two probes are loaded. In practice, the outer annulus of the accessible region is reachable only in the two-probe configuration; the full three-probe assembly is constrained to a somewhat smaller central region. Experimenters targeting cortical sites near the edge of the chamber footprint should therefore plan to operate in two-probe mode for those sessions, or use the six-probe fixture.

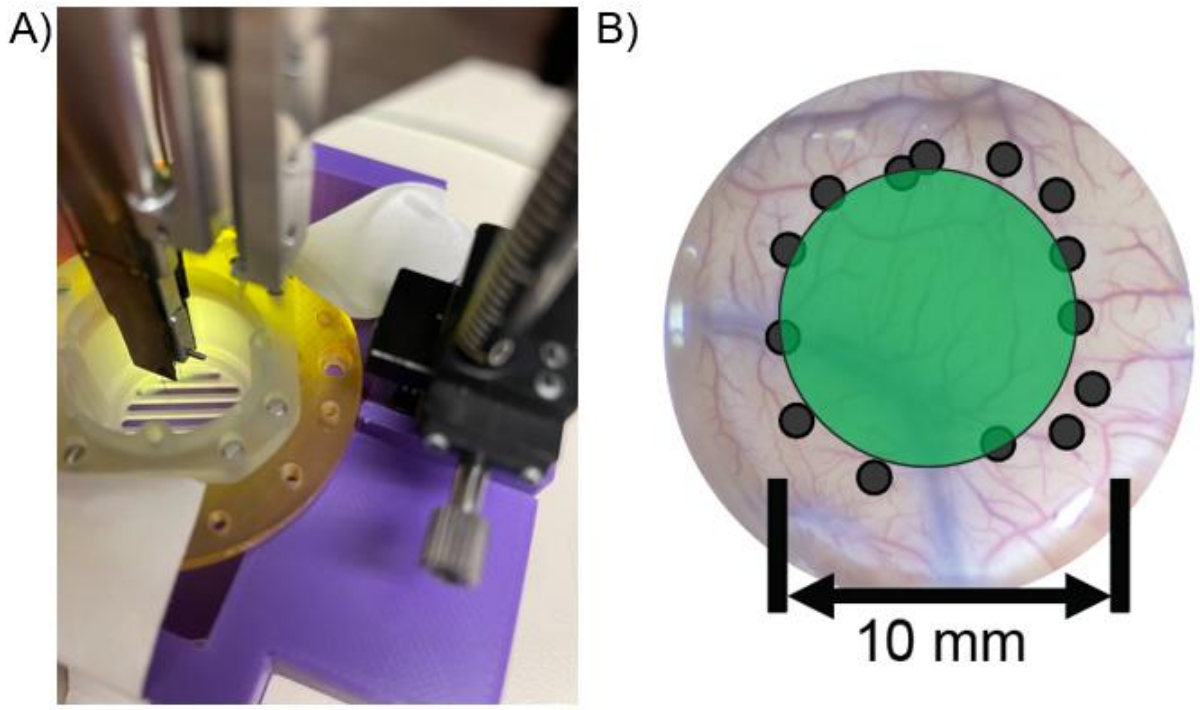

Figure 12 Dry fit testing with the three probe fixture. (A) Example insertion of fixture with two probes at the edge of the chamber. (B) Location of extreme insertions shown superimposed upon a chamber with grey circles, and total reachable area shown in green

5.2 Electrical Characterization

Electrical isolation between probes was assessed using a saline bath paradigm designed to detect inter-probe crosstalk across the frequency range of interest for neural recording. Two probes were loaded onto each fixture, and each probe was immersed in a separate saline cup with no electrical connection between the cups. A test signal was injected into one cup while the other was held at ground. Coherence between the signal probe and the grounded probe was then measured as an index of electromagnetic coupling. If the probes were well isolated, the grounded probe should show no coherence with the injected signal except at frequencies dominated by environmental noise. Data were collected for approximately 30 seconds per condition.

The test signal was a composite sinusoid spanning a range of behaviorally and electrophysiologically relevant frequencies and amplitudes. The signal sweeps across four frequencies spanning three decades — from 2 Hz in the low-frequency local field potential range through 1024 Hz in the high-frequency spiking band — and across three amplitude levels spanning two orders of magnitude, providing a comprehensive characterization of crosstalk across the relevant signal space.

Coherence was computed between all channel pairs, and the five most correlated pairs were highlighted to identify any systematic coupling. This worst-case selection is conservative: if the five highest-coherence pairs do not show stimulus-locked structure, lower-ranked pairs almost certainly do not either.

5.2.1 Three-probe electrical characterization

For the three-probe fixture, probes were placed at the two outermost positions — the back-to-back slots of the primary body — representing the configuration with the greatest potential for inter-probe cable coupling given the proximity of their headstages. Coherence between the signal probe and the grounded probe remained near zero across the full frequency range, with the only clear deviations occurring at 60 Hz and its harmonics. These deviations are attributable to environmental line noise common to both probes rather than to inter-probe coupling, as they are present at equal magnitude in probe pairs with no injected signal. No stimulus-locked coherence was detected at any of the injected test frequencies or amplitudes. The three-probe fixture therefore meets the electrical isolation requirement established in Section 3.1 across the tested signal range.

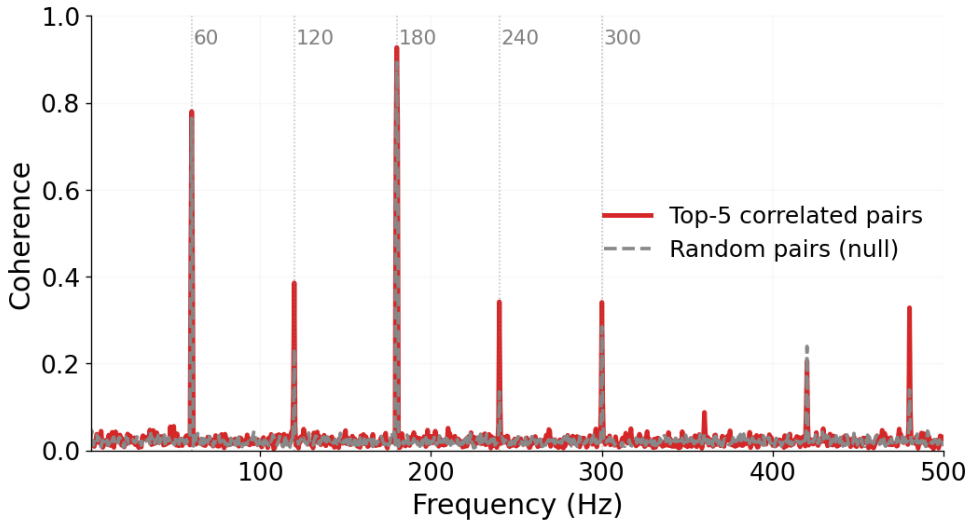

Figure 13 Frequency vs Coherence for three-probe fixture saline testing

5.2.2 Six-probe electrical characterization

For the six-probe fixture, probes were placed at the two outermost positions of a single half — a diagonal arrangement that represents the largest within-half separation available — chosen to assess whether angle had an effect on cross-talk. As with the three-probe fixture, coherence between the signal probe and the grounded probe remained near zero across all tested frequencies and amplitudes, with deviations limited to 60 Hz harmonics attributable to line noise. No stimulus-locked crosstalk was detected. The six-probe fixture therefore also meets the electrical isolation requirement, with the structural partitioning between probe mounts providing adequate electromagnetic separation even across the closer inter-probe distances imposed by the full-aperture geometry.

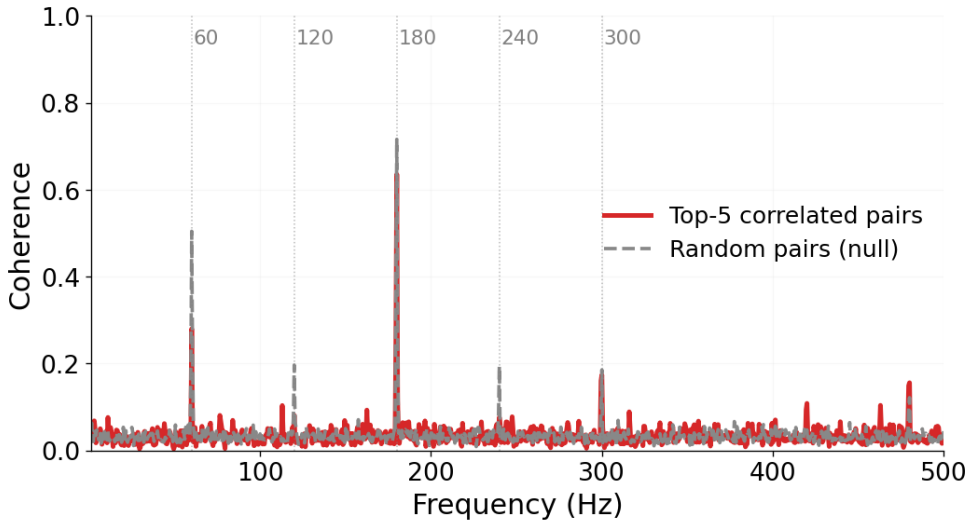

Figure 14 Frequency vs Coherence for six-probe fixture saline testing

5.3 Assembly Usability Assessment

The custom assembly jigs described in Section 4.5 were evaluated against unassisted assembly to quantify their effect on probe breakage rate and assembly time. Testing used dummy Neuropixels probes throughout to allow for direct comparison without risk to functional hardware.

Among experienced users, unassisted assembly resulted in four dummy probes broken across three assembly attempts, all attributable to screwdriver slippage during the clamping screw step — the same failure mode the jigs were specifically designed to address. With jigs in place, zero probes were broken across the equivalent operations. Assembly time was approximately halved with jigs compared to unassisted assembly, consistent with the reduction in error recovery and repositioning overhead.

Two naïve users were also evaluated, each performing one jig-assisted and one unassisted assembly in counterbalanced order. User A completed unassisted assembly first, breaking four probes, then completed jig-assisted assembly with zero breakages and reduced assembly time.

User B completed jig-assisted assembly first, breaking three probes, then completed unassisted assembly with seven breakages and longer assembly time. The ordering effect observed in User B — more breakages in the second, unassisted attempt despite having prior exposure to the task — is consistent with the jig removing a systematic mechanical hazard rather than simply providing a learning scaffold: experience with the jig did not transfer to safer freehand performance, suggesting that the screwdriver guidance it provides is not readily internalized as a manual skill.

Taken together, these results indicate that the assembly jigs substantially reduce probe breakage risk and assembly time for both experienced and naïve users, and that the reduction in breakage is not attributable to practice effects alone. Routine use of the jigs during all assembly operations is therefore strongly recommended.

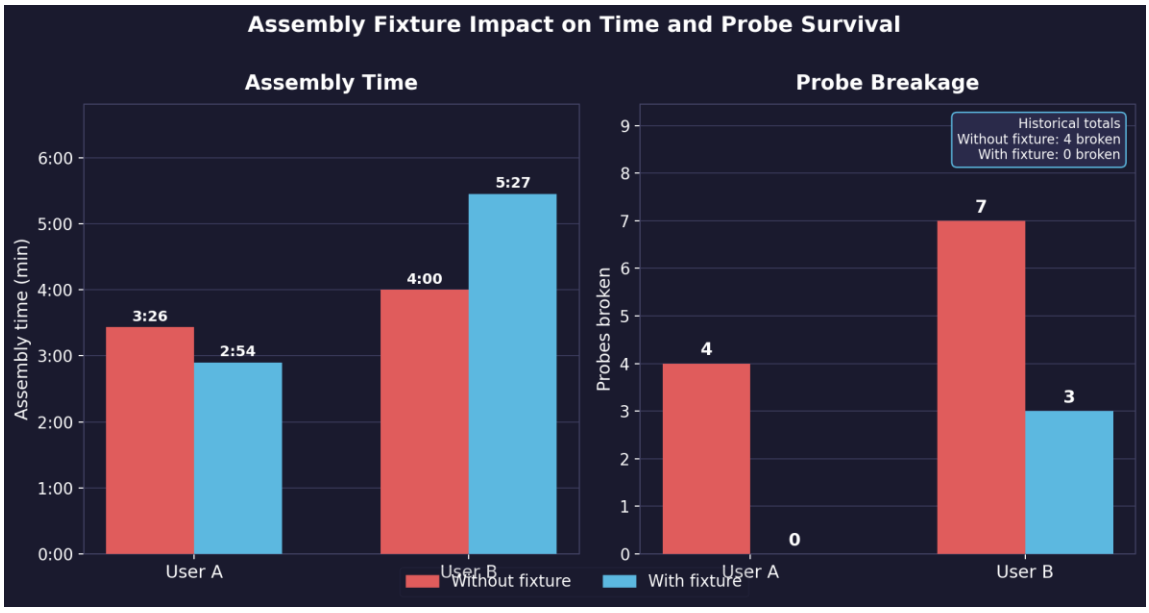

Figure 15 Assembly Fixture Impact on Time and Probe Survival

Chapter 6: Phantom Trajectory Testing

Characterizing the physical trajectories of Neuropixels probes during insertion is essential for understanding the relationship between planned and actual probe placement. While atlas-based targeting provides predicted trajectories, the extent to which probe curvature, inter-probe mechanical interaction, and surface geometry affect realized insertion paths cannot be assessed from targeting alone. This chapter describes a phantom-based testing approach developed to visualize probe trajectories directly, characterize track geometry as a function of probe straightness and fixture configuration, and assess the effect of realistic brain surface curvature on insertion behavior.

6.1 Testing Setup Design

A custom testing apparatus was designed to hold a Narishige microdrive adjacent to a block of phantom material in a configuration compatible with optical imaging during insertion. The requirement for imaging access drove the primary design constraint: at least one face of the phantom volume needed to be optically clear and accessible. A secondary design goal was generalizability — by anchoring the apparatus to a standard Narishige drive interface, the same setup can accommodate future fixture designs and syringe-based diffusion experiments that share the same drive platform.

The apparatus was designed as an open-topped box with a screw interface on the rear face for attachment of the drive holder, and a slot on the front face into which a standard microscope slide is inserted. Phantom material is poured into the box in liquid form and cured in place; the microscope slide retains the material at the front face while providing a clear viewing window for transmitted-light or transillumination imaging during probe insertion. The box was printed in-house on a desktop printer in PLA filament.

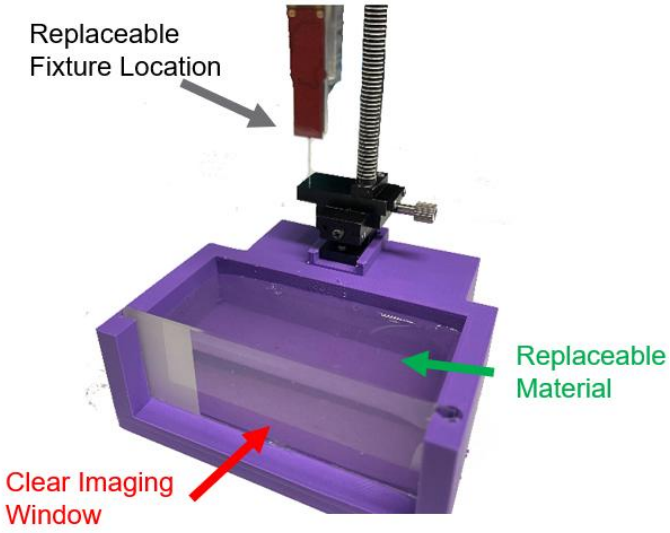

Figure 16 Testing apparatus design

6.2 Phantom Material Selection

Two candidate phantom materials were evaluated: agarose gel and ballistic gelatin. The primary selection criteria were optical clarity during insertion, the ability to retain visible dye tracks after probe retraction, and mechanical properties consistent with repeated probe insertions.

Agarose was evaluated first, motivated by the possibility of dyeing insertion tracks for enhanced visualization. A working concentration of 0.5 g ultrapure agarose powder per 20 mL water was prepared. Two dye introduction strategies were tested: coating the probe shank with food dye prior to insertion, and depositing a small volume of dye on the surface of the gel above the intended insertion site before advancing the probe. Neither approach produced reliable track staining. The only condition under which dye entered the insertion hole was direct application of a small dye droplet to the opening immediately following retraction, repeated approximately three times in succession. Even when dye entry was achieved by this method, rapid diffusion through the high water content of the agarose prevented useful track retention: the dye spread laterally within seconds, eliminating spatial specificity. Agarose blocks also exhibited significant optical cloudiness, reducing image quality during insertion. For these reasons agarose was rejected as a phantom material.

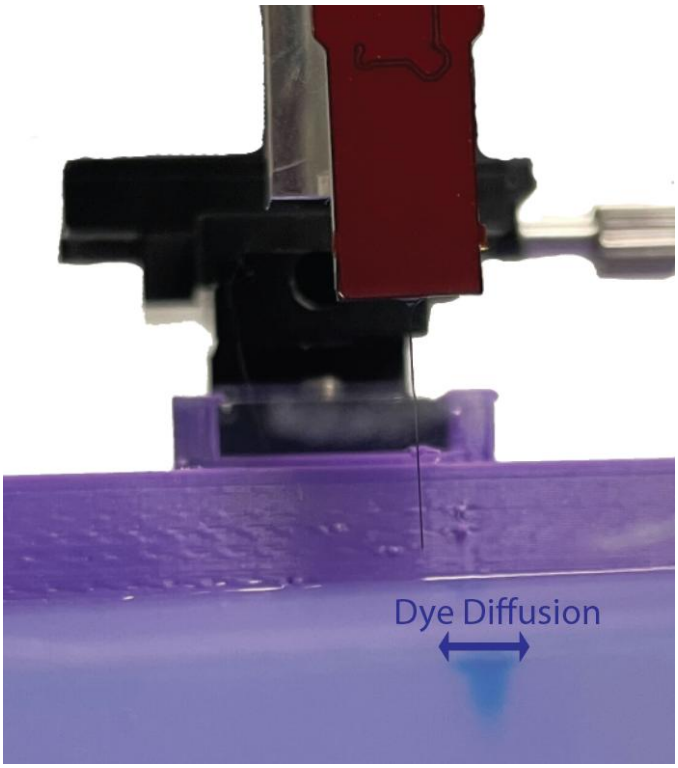

Figure 17 Single neuropixel insertion with dye into agarose block. Blue food dye diffusion is visible and labeled

Ballistic gelatin was then evaluated. As a synthetic polymer with substantially lower water content than agarose, it was expected to resist dye diffusion more effectively. In practice, ballistic gelatin proved entirely non-absorbent to food dye: only trace amounts of dye could be forced into the uppermost portion of an insertion hole, and no reliable staining of deeper track regions

was achievable. However, ballistic gelatin offered two significant practical advantages that outweighed this limitation. First, its high optical clarity allowed probe tracks to be visualized directly through the front microscope slide during and after insertion, without any staining required. Second, cured tracks could be characterized post-hoc by sectioning the gel close to the insertion site and illuminating at an oblique angle, which produced clear visualization of the track geometry under a stereo microscope. Ballistic gelatin was therefore selected as the phantom material for all subsequent testing.

As an initial characterization of single-probe track geometry, a single Neuropixels probe was inserted to a depth of 6.3 mm and retracted at the same XY location across 15 repeated insertions. Post-hoc microscopic analysis of the resulting tracks yielded a maximum track width of 0.111 mm and a maximum track length of 6.3 mm, consistent with the nominal shank width of 0.07 mm plus a small margin of tissue displacement. The close correspondence between track length and insertion depth confirmed that the phantom material did not undergo substantial compression or rebound during insertion, making depth estimates from drive readout directly interpretable as phantom penetration depth.

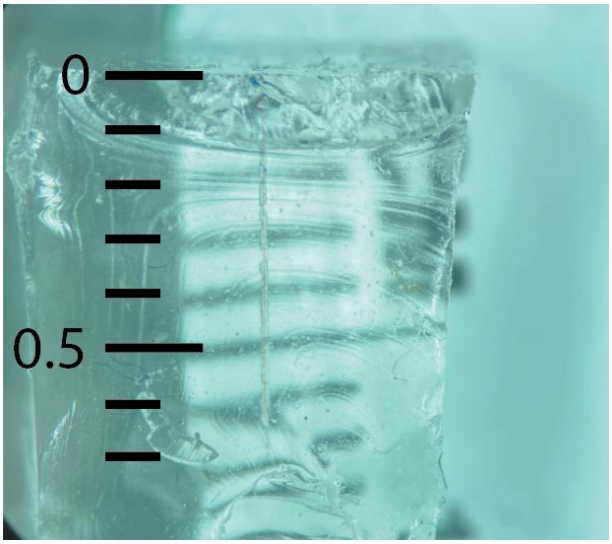

Figure 18 Single probe insertion tracks in ballistic gel. Probe was inserted 15 times in the same location.

6.3 Three-Probe inter-probe separation and curvature

Single-probe testing established that probe straightness — the degree to which the shank deviates from a true linear trajectory — has a visible effect on track width: a straight probe produces a

narrow, well-defined track, while a curved probe traces a wider path as its tip sweeps laterally during insertion. This effect is subtle with a single probe but becomes much more apparent when multiple probes are loaded simultaneously, as the divergent trajectories of adjacent probes produce visible differences in both track geometry and inter-probe separation at depth.

To characterize this effect in the three-probe fixture, three probes were selected that spanned a range of visual straightness: one probe assessed as highly straight by visual inspection, one assessed as noticeably crooked, and one assessed as intermediate. The nominal center-to-center probe spacing for the three-probe fixture is 4.8 mm. When the three selected probes were loaded and inserted, measured inter-probe distances at depth were as small as 3.75 mm — a deviation of more than 1 mm from the designed spacing — consistent with lateral displacement of the crooked probe's tip toward its neighbors during insertion. By comparison, two probes selected for visually straighter profiles produced inter-probe separations considerably closer to the 4.8 mm nominal value.

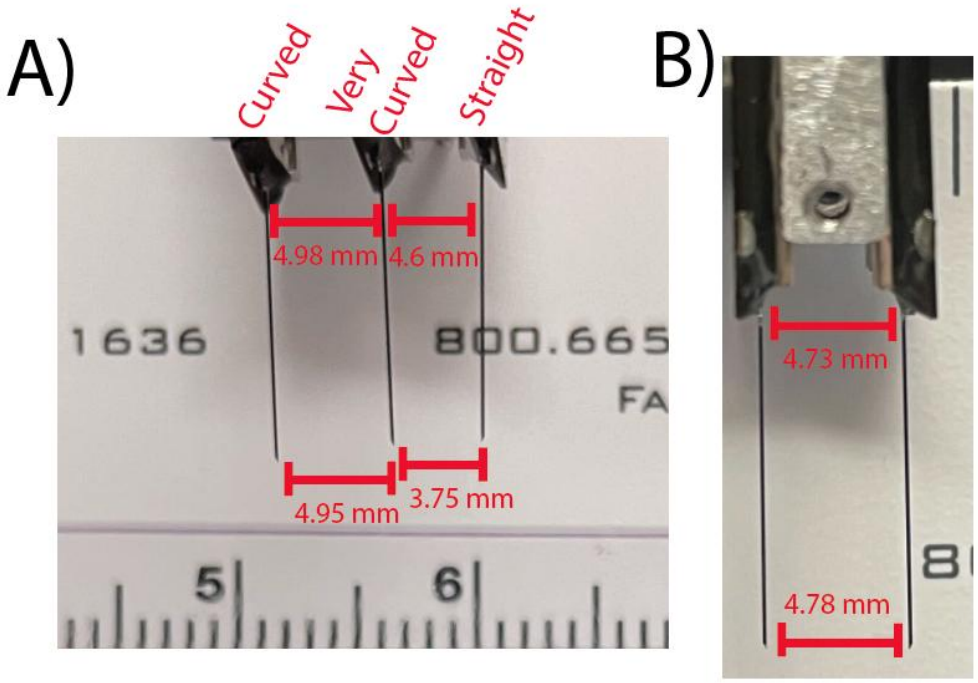

Figure 19 Probe curvature comparison. Nominal width was 4.8 mm. (A) Three probes of varying visual curvature were loaded onto the three-probe fixture. Distances of as low as 3.75 mm were measured between probes. (B) Two visually straighter probes were loaded, and maintained a much more consistent distance between probes.

Track width analysis confirmed the correspondence between visual straightness and trajectory geometry. The most curved probe produced a track 0.4 mm wide, approximately four times the single-probe baseline established in Section 6.2. The straightest probe produced a track approximately 0.1 mm wide, consistent with the single-probe baseline. The intermediate probe produced a track 0.3 mm wide. These results establish that probe-to-probe variation in shank curvature is a meaningful source of trajectory uncertainty in multi-probe configurations, and that visual pre-screening of probes for straightness prior to assembly is a practical and effective step for minimizing inter-probe displacement at depth.

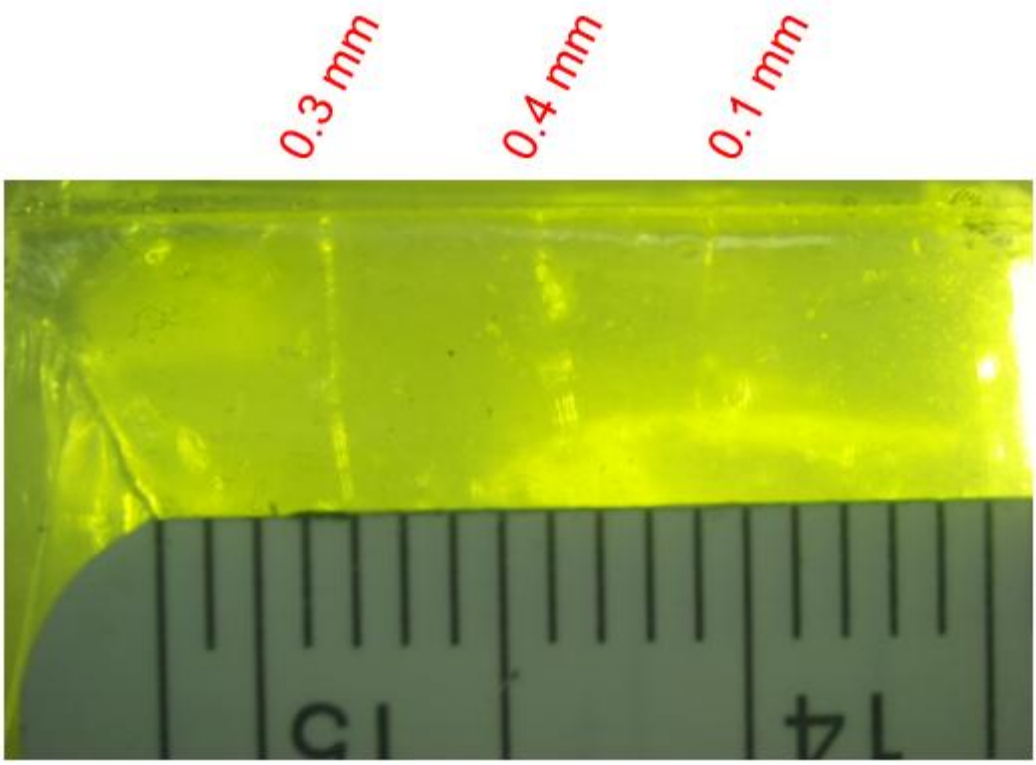

Figure 20 Track imaging of the probes from Figure 19A. Widths of track vary with curvature of probe.

6.4 Six-probe inter-probe separation and curvature

The insertion protocol from Section 6.3 was repeated with the six-probe fixture to assess whether the more constrained geometry of the full-aperture assembly introduced additional trajectory perturbations. For this test, all six probes were selected from the visually straightest available, to isolate the effect of fixture geometry from probe-level curvature variation.

Results were consistent with the three-probe findings. Each of the six probes produced tracks approximately 0.1 mm wide, matching the baseline established for straight single probes and for the straight probes in the three-probe test. No systematic broadening or deflection attributable to inter-probe mechanical interaction was observed. This indicates that loading six probes into the fixture does not itself introduce trajectory perturbation beyond that expected from individual probe properties — when straight probes are used, the six-probe fixture achieves inter-probe

separations close to the designed geometry. As with the three-probe fixture, probe straightness at assembly is therefore the primary determinant of trajectory fidelity.

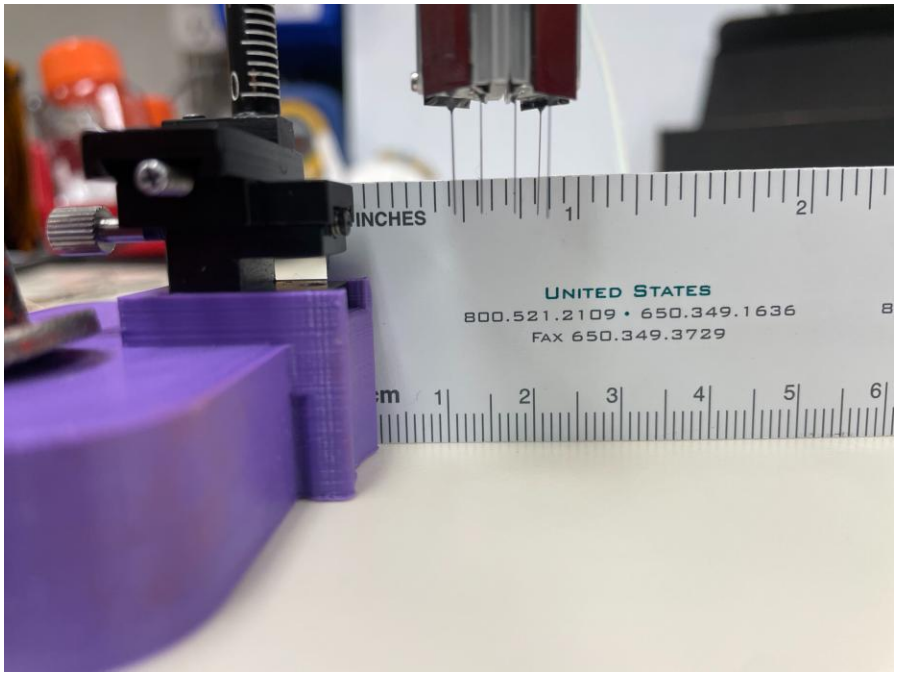

Figure 21 Probes used in insertion for six-probe verification

6.5 Brain-shaped testing

The flat phantom surface used in Sections 6.2 through 6.4 does not replicate the curved and gyrated geometry of the cortical surface encountered in vivo. Because probe trajectories are defined relative to the surface normal at the point of entry, surface curvature introduces angular variation in the effective insertion angle across probes, which may in turn affect lateral tip displacement at depth. To assess this effect, a brain-shaped phantom was prepared by casting ballistic gelatin in a model brain mold, reproducing the gross curvature and sulcal topography of the cortical surface at the relevant spatial scale.

Initial testing was performed with the brain-shaped phantom enclosed within skull and chamber models, replicating the full implanted geometry [30]. However, the enclosed configuration substantially restricted optical access and made imaging during insertion impractical. The brain-

shaped phantom was therefore sectioned to expose a cross-section near the intended insertion region, and the cut face was placed against the microscope slide window of the testing apparatus, allowing the same imaging approach used in flat-surface testing.

With the brain-geometry phantom in place, probes were observed to curve less than in the flat-surface configuration under equivalent insertion conditions. In flat conditions, the probes had distances of 5.7 and 1.8 mm. In the brain shaped conditions, the probes had distances of 4.3 mm and 2.5 mm, which is a greatly reduced amount of curvature.

This finding is consistent with the expectation that the sloped entry angle imposed by a curved surface introduces a component of lateral force that partially counteracts the probe's intrinsic curvature, reducing net tip displacement relative to the vertical. The practical implication is that flat-phantom measurements of track width and inter-probe deviation represent a conservative upper bound on the trajectory error expected in vivo: actual cortical insertions, where surface curvature is present, may yield tighter probe placement than the flat-surface phantom results suggest.

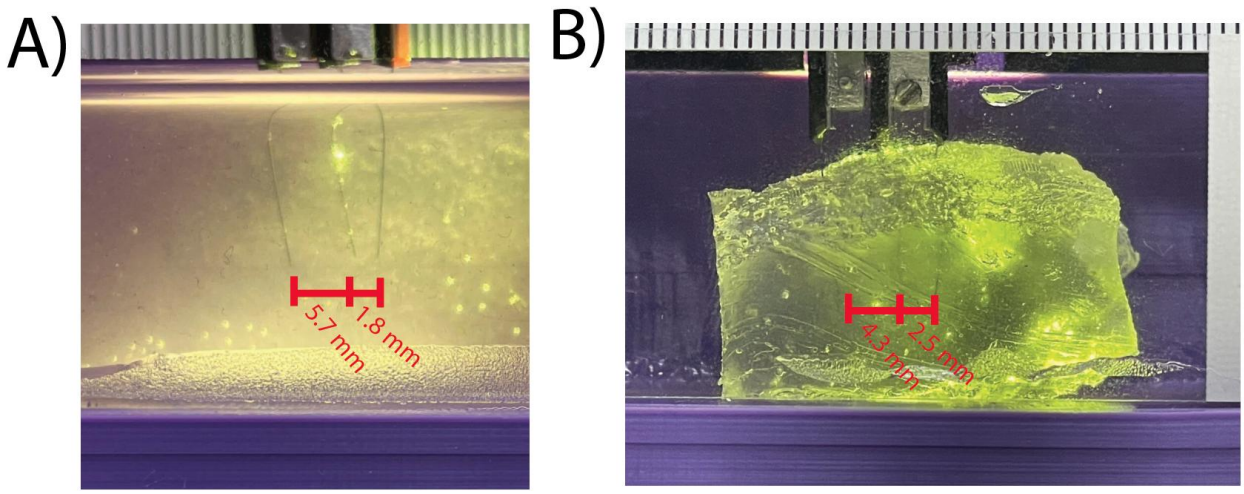

Figure 22 . Images of probes from Figure 19A during insertion. (A) Insertion was performed in a flat surface phantom, and yielded distances as low as 1.8 mm between probes (nominal is 4.8) (B) Insertion was performed in a brain shaped phantom, and yielded distances as low as 2.5 mm.

Chapter 7: Software and Computational Tools

Stereotaxic probe placement in non-human primates depends on the accurate translation of neuroanatomical targets defined in a reference atlas into physical coordinates accessible through a surgically implanted recording chamber. This chapter describes StereoPlan, the software tool introduced to address the lack of Neuropixel trajectory planning tools for NHPs.

7.1 Neuroanatomical Data Sources and Atlas Integration

7.1.1 The NIMH Macaque Template

StereoPlan is built around the NIMH Macaque Template version 2.0 symmetric, a population-averaged, skull-stripped T1-weighted MRI volume derived from scans of 31 adult rhesus macaques (Macaca mulatta) [31]. The template is distributed in NIfTI format at 0.5 mm isotropic resolution and provides a high-signal-to-noise anatomical reference that is free of individual subject idiosyncrasies. At startup, the skull-stripped image (NMT_v2.0_sym_SS.nii.gz) and its accompanying brain mask (NMT_v2.0_sym_brainmask.nii.gz) are loaded via the nibabel library and cast to 32-bit floating point. Voxels outside the brain mask are zeroed to suppress skull signal before any visualization or sampling step.

The template's affine transformation matrix encodes the mapping from voxel indices to millimeter coordinates in the standard NMT space. StereoPlan additionally applies a fixed rigid-body correction — a small rotation of [0°, 2°, −20°] in Euler XYZ convention combined with a translation of [−8, −10, −13] mm — to align the template to the stereotaxic coordinate frame used in the laboratory. The product of this correction matrix and the original NIfTI affine forms the augmented affine aff_aug whose inverse (inv_aug) is precomputed and used for all

subsequent world-to-voxel conversions, ensuring a single consistent coordinate system throughout the session.

7.1.2 The CHARM Cytoarchitectonic Atlas

Anatomical labelling is provided by the Cortical Hierarchy Atlas of the Rhesus Macaque, which parcellates the NMT space into hierarchically organized brain regions across six levels of granularity (level 0 = coarsest, level 5 = finest) [32]. The atlas is stored as a 5-D NIfTI volume (CHARM_in_NMT_v2.0_sym.nii.gz) whose fourth dimension indexes parcellation level. At startup, a single level is extracted — defaulting to level 4, which offers a practical balance between anatomical specificity and the number of distinguishable regions — and stored as a 3-D integer label volume (charm_labels) co-registered with the MRI template.

Human-readable region names and standard abbreviations are loaded from the accompanying comma-separated key table (CHARM_key_table.csv) by parsing each row with a regular expression that extracts the integer identifier, full region name, and abbreviation for the selected hierarchy level. These are stored in a module-level dictionary and accessed throughout the application via the get_label_name() function. The combination of volumetric label data and a named lookup table means that every anatomical query — whether sampling along a single probe trajectory or computing a population reach map across all chamber entry points — returns human-interpretable region identities.

7.1.3 Brain Surface Reconstruction

To support three-dimensional visualization, a polygonal mesh of the brain surface is extracted at startup using the marching-cubes algorithm as implemented in scikit-image. The MRI volume is first downsampled by a factor of two in each dimension to reduce computation time, and an

intensity threshold at the 30th percentile of in-brain signal is applied as the isosurface level. Vertex coordinates are subsequently rescaled to the full-resolution voxel grid and projected into world space via the NIfTI affine, then transformed by the stereotaxic correction matrix. The resulting surface is stored as a pyvista PolyData object and rendered as a static, non-pickable mesh throughout the session.

7.2 Probe Targeting and Reach Algorithms

7.2.1 Chamber Geometry and Coordinate System

All targeting computations are mediated by a mutable state object, `ChamberState`, which acts as the single source of truth for the physical recording chamber. The chamber is modelled as a circular aperture of user-specified radius, centered at a user-specified point in stereotaxic space, with an axis normal vector defining the probe insertion direction. Five geometric degrees of freedom are exposed to the user: three translational (X, Y, Z position of the aperture center), one radial (aperture radius), and three rotational (pitch, yaw, and in-plane roll of the insert).

The chamber's probe direction is taken as the negation of its outward normal vector. Pitch and yaw tilts are applied by computing a right-hand orthonormal frame from the base normal and rotating it using Rodrigues' rotation formula as implemented in `scipy.spatial.transform.Rotation`. Roll (in-plane rotation of the grid insert) is applied separately as a rotation of the hole-center positions around the chamber normal axis after the grid pattern has been computed, leaving the probe direction unchanged.

When the chamber center is repositioned via `set_center()`, pitch, yaw, and roll are automatically reset to zero, ensuring that tilt angles always reflect deviations from the base orientation at the current anatomical location rather than accumulating across moves. When any geometric

parameter is modified, the `rebuild()` method recomputes all dependent geometry: the filled aperture disc mesh used for three-dimensional visualization and point picking, the torus-shaped chamber ring, and the flat disc entry grid that seeds the dense-mode reach computation. All meshes are constructed analytically from the current center, normal, and radius, with no dependence on cached state from previous configurations.

7.2.2 Grid Insert Modeling

Physical recording chambers are typically used with standardized grid inserts that constrain probe entry to a discrete pattern of holes. StereoPlan implements two Orsborn Lab inserts as well as a user-configurable custom grid.

The first insert uses two interleaved hole populations arranged on 2 mm row and column spacing: seven rows of 3, 5, 7, 7, 7, 5, and 3 holes with a 0.55 mm hole radius, interspaced with six rows of 5 holes each with a 0.454 mm hole radius, yielding a 67-hole pattern. The second insert uses 1.52 mm spacing throughout: ten rows of 2, 6, 8, 8, 10, 10, 8, 8, 6, and 2 holes with a 0.454 mm hole radius, interspaced with nine rows of 5, 7, 9, 9, 9, 9, 9, 7, and 5 holes with a 0.375 mm hole radius, yielding 137 holes. Both inserts are implemented as builder functions (`_build_crist_a`, `_build_crist_b`) that compute hole centers in the chamber's local orthonormal frame and project them into world space via a shared `_rows_to_world()` helper. The Custom preset generates a simple square grid with user-specified hole spacing and radius.

Hole center positions are computed in the chamber's local orthonormal frame (spanned by vectors *u* and *v* perpendicular to the probe normal) and projected into world space. After any in-plane roll rotation is applied, holes whose centers lie at a distance greater than (chamber_radius −

hole_radius) from the aperture center are discarded, preventing the physical insert from overhanging the chamber rim.

The grid insert is also represented visually in the three-dimensional viewport. A semi-transparent plate disc is rendered as a backdrop, and each hole is rendered as a torus-shaped rim mesh. For performance, all hole rim meshes are merged into a single VTK actor before rendering. Pickable hole-center spheres — also merged into one actor — allow the user to select entry points by clicking in the viewport.

7.2.3 Single Probe Placement

In 'Place Probe' mode (Tab 1), the user clicks a point on the three-dimensional viewport. The application resolves the clicked point to the nearest valid entry location: in grid-insert mode, this is the closest hole center within two hole-radii of the picked point; in open-disc mode, it is the projection of the picked point onto the aperture plane. Once an entry point is established, the maximum insertable depth is determined by stepping along the probe direction in 0.25 mm increments and testing each position against the brain-mask volume via the `world_to_vox()` coordinate transform, stopping when the trajectory exits the mask. The resulting depth is clamped to a minimum of 1 mm. The probe is visualized as a red line from entry to tip, with the

depth interactively adjustable via a slider.

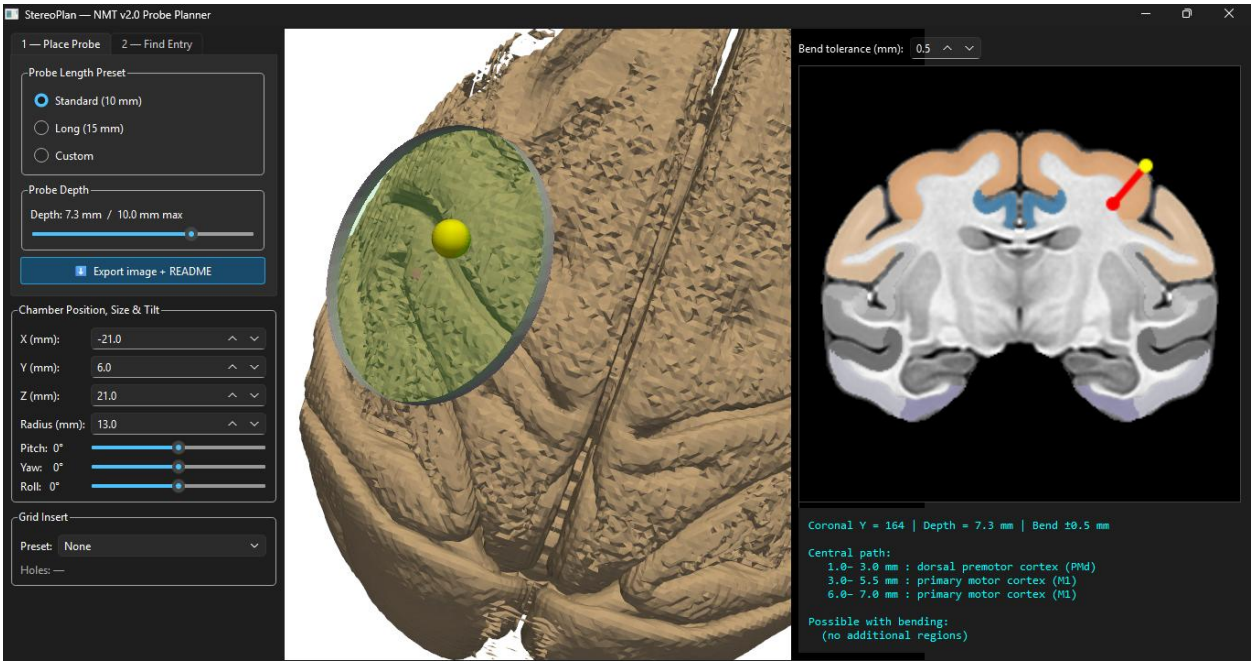

Figure 23 Example placement of a probe in tab 1

Along the current trajectory, anatomical labels are sampled at 0.5 mm intervals using `sample_charm_along_probe()`. Consecutive samples sharing the same label identifier are merged into contiguous segments, each annotated with its start depth, end depth, and region name. This segment list is displayed in the coronal panel and forms the basis of the tissue-sequence section of exported planning documents.

7.2.4 Bend-Tolerance Cylinder Sampling

The coronal anatomy panel exposes a bend-tolerance control that models the worst-case volume a probe could occupy given lateral deflection during insertion. The `sample_charm_cylinder()` function sweeps a cylinder of user-specified radius (default 0.5 mm, adjustable from 0 to 5 mm in 0.1 mm steps) around the probe axis, sampling CHARM labels at every depth step on the central ray and at concentric rings of radial offset points (3 rings, 12 sectors each). The function

returns two values: the central-ray segment list identical to `sample_charm_along_probe()`, and the full set of non-zero label identifiers encountered anywhere within the cylinder.

Labels within the cylinder but absent from the central ray are reported in the coronal panel under a separate 'Possible with bending' heading. The bend envelope is also rendered visually as a semi-transparent red polygon around the probe line in the coronal view, providing an intuitive representation of the spatial uncertainty introduced by probe deflection. This feature allows users to identify anatomical structures that lie close to the planned trajectory and might be inadvertently contacted if the probe deflects.

7.2.5 Population Reach Analysis and Heatmap Computation

The 'Find Entry' tab (Tab 2) addresses the inverse problem: given a target brain region, which entry points in the chamber can reach it? This is implemented as a batched, fully vectorized computation that avoids Python-level loops over entry points.

For a user-selected target label, the algorithm constructs the complete set of probe sample points for all N entry positions simultaneously. If there are N entries and S depth steps from 0.5 mm to the configured maximum in 0.5 mm increments, this yields an (N × S × 3) array of world-space coordinates. A single matrix multiplication against the pre-inverted augmented affine converts the entire array to voxel indices in one operation. An in-bounds mask is then applied, and the CHARM label volume is indexed with NumPy fancy indexing to retrieve an (N × S) array of region identifiers. For each entry row, the shallowest depth step at which the target label is encountered is recorded as the reach depth; entries with no matching sample receive a depth of zero. This approach reduces the computational complexity from O(N×S) Python iterations to a

small number of array operations, yielding substantial speed improvements over an equivalent loop-based implementation, particularly for the 137-hole insert.

The resulting depth array is cached against the target label identifier and reused without recomputation unless the chamber geometry changes. Heatmap results are visualized in the three-dimensional viewport. In grid-insert mode, each hole-center sphere is colored according to reach depth using a red-yellow-green diverging colormap (`RdYlGn_r`), with grey used for entries that cannot reach the target; all spheres are merged into a single actor for rendering efficiency. In open-disc mode, a Delaunay-triangulated surface is computed over the entry grid and colored by reach depth, supplemented by individual spheres at a subsampled set of reachable points. The sorted list of reachable entries, together with their grid hole identifiers and reach depths, is presented in a tabular format in the Find panel.

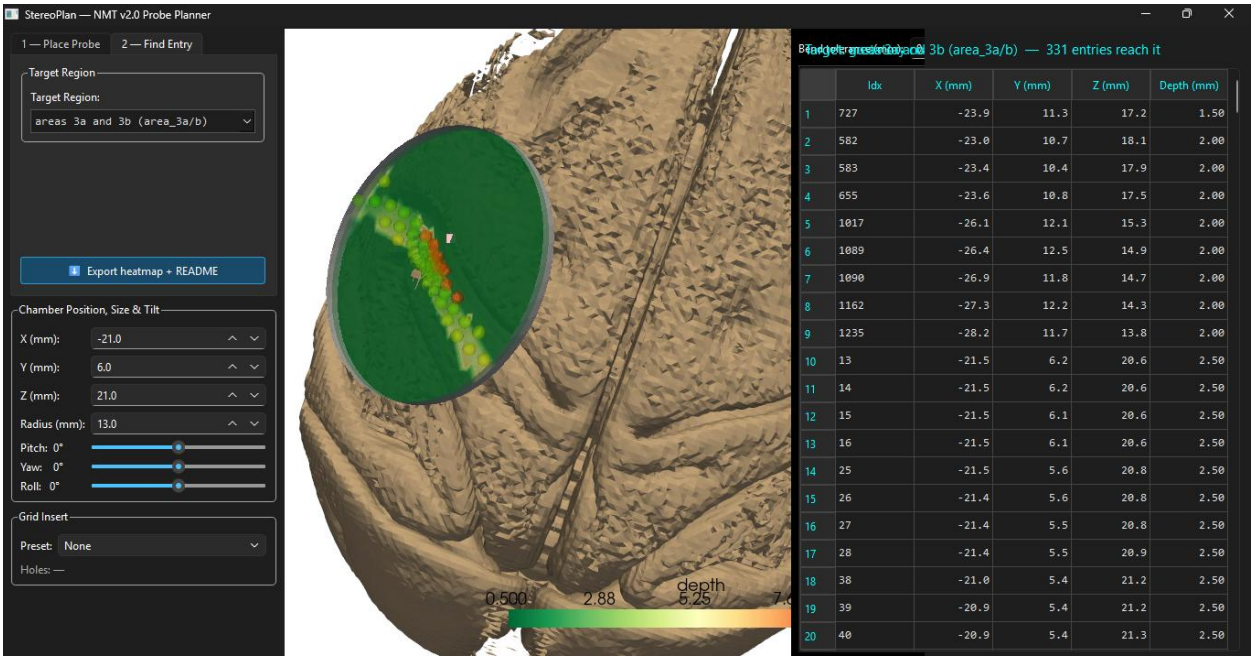

Figure 24 Example heatmap and reachable entries table for a target region in tab 2

7.2.6 Reachable Region Enumeration

When the chamber is repositioned, StereoPlan recomputes the set of brain regions reachable from any point in the current grid. This is implemented by `compute_reachable_labels()`, which walks trajectories from the chamber center and from every tenth entry point in the grid, collecting all non-zero label identifiers encountered. The union of these sets forms the reachable label list, which is sorted and used to populate the region dropdown in the Find Entry tab. This approach deliberately samples sparsely (every tenth entry) to remain interactive while still capturing the broad anatomical footprint of the chamber position.

When the Find Entry tab is active and the chamber moves, the previously selected region is preserved in the dropdown if it remains reachable from the new position. If it is no longer reachable, the selection defaults to the first available region. The reachable label list is also computed once at module startup from the default chamber position, so the dropdown is populated immediately without requiring a chamber move.

7.3 User Interface Design

7.3.1 Framework and Layout

The graphical interface is implemented using PySide6, the official Python binding for the Qt 6 framework. The main window comprises three horizontal panels: a left-hand controls column (300 px fixed width), a central three-dimensional viewport (700 px fixed width), and a right-hand context panel (500 px fixed width) that switches between the coronal anatomy view and the Find Entry table depending on the active workflow tab. The window opens in a maximized state to fill the available display area without entering a full-screen mode that would suppress the operating system taskbar.

The three-dimensional viewport is provided by PyVista's Qt interactor (`QtInteractor`), embedded directly in the PySide6 widget hierarchy. PyVista is a high-level wrapper around the Visualization Toolkit (VTK) that exposes mesh rendering, actor management, and point-picking through a Python API. The brain surface, chamber geometry, and probe actors all live as VTK actors within this interactor and are updated in-place when parameters change.

7.3.2 Tab 1 — Place Probe

The first workflow tab supports manual probe placement. A radio-button group allows selection among preset probe lengths (10 mm labelled 'Standard', 15 mm labelled 'Long') or a user-specified maximum entered via a spin box, controlling the upper bound of the depth slider. The custom-length spin box is only shown when the Custom radio button is selected. A horizontal slider spanning the full probe length range (in 0.1 mm increments) allows post-placement adjustment of insertion depth, with the three-dimensional visualization updating in real time. The depth label displays both the current depth and the active maximum (e.g., 'Depth: 6.0 mm / 10.0 mm max'). Point picking is enabled on the three-dimensional viewport; clicking any pickable surface (the aperture disc in open mode, or hole spheres in grid mode) triggers trajectory resolution and probe rendering as described in Section 7.2.3.

An export button at the bottom of the tab invokes the planning export function, which captures the current three-dimensional viewport screenshot, composites it with the coronal anatomy panel, and writes a timestamped PNG image and a plain-text README file to a user-chosen directory (see Section 7.4).

7.3.3 Tab 2 — Find Entry

The second workflow tab provides the target-driven entry search. A dropdown menu lists all brain regions reachable from the current chamber position, identified by their full CHARM name and abbreviation. Selecting a region triggers heatmap computation (or retrieval from cache) and updates both the three-dimensional viewport and the Find panel on the right. The Find panel displays a scrollable table of all entries that can reach the selected region, sorted by ascending depth and labelled with hole identifiers (in grid mode) or Cartesian coordinates (in open-disc mode). Clicking a table row sets the active probe to that entry and depth, updating the coronal view accordingly.

In grid-insert mode the Find panel table shows four columns: hole identifier (formatted as H000), X and Y coordinates in the chamber plane, and reach depth in millimeters. In open-disc mode a fifth column showing the Z coordinate is added, and entries are identified by index rather than hole label. The title bar of the Find panel displays the target region name and the number of entries that can reach it.

When the Find tab is active and the user clicks an entry point in the three-dimensional viewport, the probe depth is set to the heatmap reach depth for that hole (if a target label is selected and the hole reaches it), rather than the maximum brain-mask depth used in the Place Probe tab.

The region list is recomputed whenever the chamber is moved and the dropdown is repopulated automatically, preserving the previously selected region if it remains reachable from the new position. A separate export button produces a heatmap composite image and README analogous to the Tab 1 export.

7.3.4 Chamber and Insert Controls

Below the workflow tabs, a 'Chamber Position, Size & Tilt' group box exposes six controls: spin boxes for the X, Y, and Z coordinates and radius of the chamber aperture, and sliders for pitch (−45° to +45°), yaw (−45° to +45°), and roll (−180° to +180°). Pitch and yaw tilt the probe insertion direction relative to the base normal, while roll rotates the grid insert pattern in the aperture plane without altering the trajectory direction, enabling the user to align insert row and column axes with anatomical structures of interest.

All chamber parameter controls employ a 180 ms debounce timer: the three-dimensional geometry is not recomputed on every incremental slider tick, but only after the user pauses for at least 180 ms. Separate debounce timers are maintained for chamber position/radius changes, tilt (pitch/yaw) changes, and roll changes, so that adjusting one axis does not cancel a pending update on another. This prevents the application from queuing many redundant full rebuilds during rapid slider movement while remaining subjectively responsive.

A 'Grid Insert' group box below the chamber controls provides a dropdown for selecting the insert preset (None, Crist A, Crist B, or Custom) and, when Custom is selected, spin boxes for hole spacing and hole radius. A read-only label below the dropdown displays the current hole count, updating automatically when the preset or chamber geometry changes. When a non-custom preset is selected, the spacing and radius spinboxes are updated to reflect the preset's actual parameters.

7.3.5 Coronal Anatomy Panel

The right-hand panel in Tab 1 mode displays a coronal slice through the MRI template at the anterior-posterior coordinate of the current probe entry point. The MRI is rendered as a greyscale

image with the CHARM parcellation overlaid at 65% opacity using the tab20c colormap, providing simultaneous anatomical and parcellation context. The probe is drawn as a red line with a yellow entry marker and a red tip marker. The panel recalculates and redraws on every depth-slider change.

The bend-tolerance corridor is drawn as a semi-transparent red polygon around the probe line whenever the bend radius is greater than zero. The panel caches the last probe entry, direction, and depth so that changes to the bend-tolerance spinbox can trigger a re-render without requiring a new point pick. The panel also responds to window resize events, rescaling the cached full-resolution pixmap to fit the available space while preserving aspect ratio.

7.4 Data Inputs and Outputs

7.4.1 Inputs

StereoPlan requires four input files, all specified as absolute paths in the configuration section of the core module:

- NMT_v2.0_sym_SS.nii.gz — skull-stripped T1-weighted template MRI (NIfTI)
- NMT_v2.0_sym_brainmask.nii.gz — binary brain mask in template space (NIfTI)
- CHARM_in_NMT_v2.0_sym.nii.gz — multi-level cytoarchitectonic parcellation (5-D NIfTI)
- CHARM_key_table.csv — region name lookup table (CSV)

All four files are distributed as part of the NMT v2.0 release package and require no preprocessing before use. At startup, all volumes are loaded into RAM in their entirety; the template MRI occupies approximately 50 MB at 32-bit precision, the brain mask approximately 12 MB, and the CHARM label volume (single level) approximately 12 MB as a 16-bit integer

array. Total memory demand at initialization is therefore modest by the standards of neuroimaging software.

7.4.2 Session State

There is no persistent session file format. All planning state — chamber position, insert selection, probe placement, and heatmap cache — is held in memory for the duration of a session. If the user closes the application, parameters must be re-entered from notes or from exported planning documents. This is a known limitation of the current implementation and a candidate for future development.

7.4.3 Exports

StereoPlan provides structured exports from both workflow tabs. Each export produces two files, timestamped to the nearest second to prevent overwriting:

- Composite PNG image. The image is constructed programmatically using Qt's QPainter API. For Tab 1 exports, the layout places the three-dimensional viewport screenshot (captured via PyVista's screenshot() method) on the left and the coronal anatomy panel on the right, with a metadata text panel beneath both. For Tab 2 exports, the three-dimensional heatmap view occupies the left panel and a rendered entry table occupies the right, again with a metadata panel below. All panels are composited onto a dark background. Files are named stereoplan_place_YYYYMMDD_HHMMSS.png or stereoplan_find_YYYYMMDD_HHMMSS.png as appropriate.
- Plain-text README. A structured plain-text file records all planning metadata relevant to the export. For Tab 1, this includes: chamber center and radius; chamber normal vector; pitch, yaw, and roll angles; grid preset name and hole count; probe entry and tip coordinates; total insertion depth; and the full tissue-region sequence with millimeter ranges. For Tab 2, it includes the same chamber metadata plus the target region name, the summary statement from the Find panel, and the complete sorted entry table with hole identifier (or index), Cartesian coordinates, and reach depth. Files are named stereoplan_place_YYYYMMDD_HHMMSS_README.txt or stereoplan_find_YYYYMMDD_HHMMSS_README.txt.

7.5 Validation of Targeting Accuracy

7.5.1 Sources of Targeting Error

Any software-guided stereotaxic targeting system operates under a set of assumptions that introduce error into the mapping between planned and actual probe positions. Understanding these sources is essential for interpreting the precision of coordinates generated by StereoPlan.

Template-to-subject registration error. StereoPlan plans trajectories in the space of the NMT v2.0 population-average template. The degree to which template coordinates correspond to anatomically equivalent locations in any given subject depends on the quality of the registration between that subject's individual MRI and the template. Population-average templates by construction minimize average deformation across subjects, but individual brains differ in sulcal geometry, brain size, and gyral pattern. Registration errors of several millimeters are plausible in regions of high inter-individual variability, particularly in prefrontal and temporal cortex.

Chamber placement error. The correspondence between the chamber's physical position on the skull and its modelled position in StereoPlan depends on the accuracy with which the chamber was implanted and the accuracy with which post-implant imaging (MRI or CT) was registered to the planning space.

Probe deflection. The software models probe trajectories as perfectly straight lines from entry to tip. In practice, probes deflect as they traverse tissue of varying mechanical stiffness, particularly when passing through white matter tracts or across the dura. This effect is more pronounced for flexible probes and longer insertion depths. The bend-tolerance cylinder sampling described in Section 7.2.4 provides a qualitative indication of which anatomical structures lie within a

specified deflection radius of the planned trajectory, but StereoPlan does not model the precise mechanics of deflection itself.

Atlas labelling uncertainty. CHARM region boundaries are derived from group-level histological data and may not correspond precisely to individual-subject cytoarchitectonic boundaries. The 0.5 mm sampling resolution of the atlas and the probabilistic nature of parcellated boundaries mean that label assignments near region borders carry inherent uncertainty. Users should treat the tissue-sequence output as indicative rather than definitive, particularly for thin cortical layers or small subcortical nuclei.

7.5.2 Internal Consistency Checks

Several properties of the software implementation can be verified for internal consistency. The coordinate transform chain — world space → augmented affine inverse → voxel space — is a bijective affine map; applying world_to_vox() and its inverse to a set of known anatomical landmarks and confirming that voxel-space positions agree with manual atlas inspection provides a basic sanity check. The probe sampling in sample_charm_along_probe() uses the same coordinate transform, so consistency between the coronal-panel anatomy overlay and the tissue-sequence readout is a further implicit check.

7.5.3 Practical Guidance for Users

Given the sources of error enumerated above, the following practical workflow is recommended for users employing StereoPlan in active experiments:

- Use the chamber's physical grid insert (matched to the preset used in software) to constrain entry to hole positions, reducing continuous positional uncertainty to the discrete set of hole centers. The software's hole-proximity picking logic ensures that planned and executed entry points are identical.

- Use the bend-tolerance feature to identify anatomical structures within the deflection envelope of the planned trajectory, and cross-reference against the tissue-sequence output to assess whether off-axis contacts are a concern for the specific recording target.
- Cross-reference the tissue-sequence output against independent electrophysiological markers where possible — characteristic multi-unit firing patterns, local field potential signatures, or the depth of dural penetration — to accumulate a site-specific empirical correction for any consistent registration offset.
- Export a planning document for each recording session before the animal is brought to the laboratory. The README and composite image together constitute an unambiguous record of the intended trajectory that can be consulted intraoperatively and archived alongside electrophysiological data.

7.6 Software Dependencies and Availability

StereoPlan is implemented in Python 3.10 or later. The core numerical and neuroimaging dependencies are listed in the table below. The graphical interface requires PySide6 6.5 or later and a system OpenGL driver supporting VTK's rendering backend.

Package	Version tested	Role
nibabel	≥3.2	NIfTI file loading and affine handling
numpy	≥1.24	Array operations and vectorised computation
scipy	≥1.10	Rotation algebra (Rodrigues, Euler angles)
scikit-image	≥0.20	Marching-cubes surface reconstruction
pyvista	≥0.42	3-D mesh representation and VTK rendering
pyvistaqt	≥0.11	Qt-embedded PyVista interactor
PySide6	≥6.5	Qt 6 GUI framework
matplotlib	≥3.7	Colormap lookup (tab20c, RdYlGn_r)

The application is structured as a set of six Python modules: core.py (data loading, geometry construction, and probe-sampling algorithms), visualization.py (three-dimensional rendering and pick handling), gui.py (main window and controls), coronal_panel.py (two-dimensional anatomy view with bend-tolerance overlay), find_panel.py (target entry table), and export_utils.py (image and text export). Entry point is main.py. The modular structure ensures that the computational core is testable independently of the graphical interface and that the visualization and GUI layers can be updated without modifying the underlying algorithms.

Chapter 8: Discussion & Conclusion

This thesis presented three complementary hardware and software contributions toward enabling large-scale, multimodal motor cortical recordings in rhesus macaques: a three-probe linear fixture for flexible session-by-session recording, a six-probe fixture with co-registered optical fibers for high-density fixed-array recording, and StereoPlan, a Python-based desktop application for atlas-guided probe trajectory planning. Electrical characterization confirmed that both fixtures achieve the inter-probe isolation required for high-fidelity neural recording. Custom assembly jigs were developed alongside the fixtures, substantially reducing probe breakage and assembly time for both experienced and naïve users. Phantom-based trajectory testing characterized Neuropixels probe behavior under realistic insertion conditions, identifying probe shank curvature as the dominant source of inter-probe separation error and demonstrating that flat-surface phantom measurements provide a conservative upper bound on in vivo trajectory deviation.

8.1 Summary of Key Findings

This thesis addressed two aims: the development and validation of scalable multi-probe Neuropixels fixtures for use in rhesus macaques, and the development of supporting computational and phantom-based tools for probe trajectory planning. Three contributions were presented: a three-probe linear fixture for session-by-session flexible recording, a six-probe fixture with co-registered optical fibers for high-density multimodal recording, and StereoPlan, a Python-based desktop application for atlas-guided probe trajectory planning in NHPs.

Phantom insertion testing established that ballistic gel is an adequate mechanical surrogate for characterizing Neuropixels trajectory consistency, though it required microscopy rather than

naked-eye inspection to resolve tracks and could not be stained by any dye tested. Single-probe insertions across 15 trials in the same location produced tracks with a maximum width of 0.111 mm and a maximum length of 6.3 mm, demonstrating highly repeatable trajectories. Three-probe testing revealed that probe shank curvature — present in individual probes but most apparent when all three are mounted together — produces inter-probe separation deviations of up to approximately 0.5 mm around the 4.8 mm nominal spacing. This is a meaningful source of targeting uncertainty that must be accounted for when interpreting recordings relative to StereoPlan predictions.

Assembly usability testing produced the clearest result: without the custom jigs, four dummy probes were broken in three assembly attempts due to screwdriver slippage; with the jigs, zero probes were broken and assembly time was reduced by approximately half.

8.2 Interpretation of Mechanical Results

The single-probe trajectory data indicates that the drive and carriage adapter mechanism produces highly consistent insertion paths across repeated trials: a maximum lateral spread of 0.111 mm over 15 insertions of 6.3 mm depth means that the drive introduces less than 0.9% lateral deviation relative to insertion depth. This is small enough that drive-induced positional error is unlikely to be the dominant source of targeting uncertainty in practice, particularly compared to the inter-subject anatomical variability that StereoPlan accounts for through atlas registration.

The inter-probe separation data presents a more significant concern. The measured spread of approximately 0.5 mm around the 4.8 mm nominal spacing is large enough to matter for laminar-resolution recording, where a 0.5 mm positional error at the tip corresponds to roughly two

cortical layers. The deviations stem from two separable sources: probe shank curvature, which is a property of the Neuropixels probes themselves rather than the fixture, and fixture fabrication tolerances. Probe curvature is most visible when probes are mounted in the same fixture precisely because the fixture provides a common reference frame against which individual curvature becomes apparent. This finding suggests that any multi-probe fixture using Neuropixels 1.0 probes will face this limitation regardless of fixture precision, and that propagating a positional uncertainty of ±0.25 mm into StereoPlan targeting estimates is appropriate when interpreting data from the three-probe fixture. Repeating these measurements with the final machined metal fixture, rather than the tape-connected prototype used here, will be needed to separate fixture-fabrication error from probe curvature as independent contributors to the total spread.

Six-probe fixture trajectory results were consistent with the three-probe findings when visually straight probes were used, with all six probes producing tracks approximately 0.1 mm wide and inter-probe separations close to the designed geometry. This confirms that the fixture geometry itself does not introduce additional trajectory perturbation beyond what is attributable to individual probe curvature. Brain-geometry phantom testing further revealed that cortical surface curvature partially counteracts probe deflection, with flat-surface phantom measurements therefore providing a conservative upper bound on expected in vivo tip displacement. Experimenters can use flat-phantom inter-probe deviation measurements as a worst-case estimate when planning multi-area recordings and interpreting post-hoc laminar position.

The dry fit testing result — that the three-probe fixture preserves the approximately 10 mm accessible footprint of the single-probe predecessor — is a direct consequence of the linear body design and validates a central architectural decision. By arranging all three probe mounts along a

single narrow axis rather than distributing them laterally, the fixture achieves multi-probe capability without sacrificing the working radius that determines which cortical areas can be targeted. The trade-off is that the linear arrangement constrains the accessible probe separation geometries: the three probe positions are collinear, which suits experiments targeting areas arranged along the rostrocaudal axis of motor cortex (e.g., PMd and M1) but is less well suited to simultaneously targeting widely separated lateral and medial areas. Experimenters whose targets do not align with the linear axis should consider using the six-probe fixture or deploying the three-probe fixture in a two-probe configuration at the edge of the chamber footprint.

The electrical isolation results confirm that the structural partitioning approach — physically separating probe mounts with interposed material and routing cables away from neighboring headstages — is sufficient to meet the isolation requirement across the full neural recording bandwidth. The absence of stimulus-locked cross-talk at any of the injected test frequencies, even at the closest inter-probe geometries tested, indicates that the fixture architecture successfully decouples the electromagnetic environments of adjacent probes. This is a non-trivial result: in the two-probe predecessor, cable proximity and headstage coupling were identified as primary noise sources that degraded recording quality. The new designs eliminate this failure mode by construction.

8.3 Interpretation of Assembly Usability Results

The assembly usability results demonstrate that the custom jigs address a genuine and repeatable mechanical hazard rather than providing merely a learning scaffold. The critical observation is the ordering effect seen in User B, who broke more probes in the unassisted condition after having first completed jig-assisted assembly — a result inconsistent with a simple learning curve

account. If the jigs were primarily beneficial as a structured practice environment, prior jig use would be expected to transfer to safer unassisted performance. Instead, the jig appears to remove a physical constraint that cannot be reliably internalized as motor skill: specifically, preventing screwdriver tip displacement during the clamping step. This interpretation is consistent with the consistent failure mode observed across all unassisted conditions (screwdriver slippage), and with the zero-breakage rate under jig-assisted conditions even for naïve users on their first attempt.

The approximately 50% reduction in assembly time with jigs is likely attributable to the elimination of error-recovery steps (repositioning the screwdriver after slippage, inspecting for damage) as well as reduced cognitive load during alignment. In a vivarium setting, where preparation time is constrained and personnel may be working under gloves and PPE, this time reduction has practical significance beyond the purely economic: shorter assembly windows reduce the opportunity for fatigue-related error during the most safety-critical stage of probe handling. Given that Neuropixels probes represent a substantial per-unit cost, routine jig use is strongly recommended, and future fixture designs should incorporate jig compatibility as a primary assembly design constraint rather than an afterthought.

8.4 Limitations and Outstanding Validation

Several important validation steps remain before the systems described here can be considered fully characterized for routine experimental use. First, neither fixture has yet been validated in vivo. In vivo validation would require deploying the fixtures in an animal with a surgically implanted chamber, confirming that probe advancement is smooth and mechanically stable, that single-unit yields are comparable to the single-probe predecessor, and that recorded units can be

localized to the intended anatomical targets using StereoPlan predictions as a reference. The six-probe fixture additionally requires in vivo validation of the optogenetic pathway: confirming that fiber placements achieve transduction volumes of sufficient extent to modulate unit activity at the intensity levels described in Section 2.5.

Second, StereoPlan's targeting accuracy has not yet been validated against a ground-truth anatomical reference in a live animal. Validation could proceed by recording characteristic electrophysiological markers (e.g., the depth of cortical layer IV in primary motor cortex, identified from current source density analysis) and comparing the observed marker depth with StereoPlan's prediction from the atlas-registered trajectory. An accumulated dataset of such comparisons across sessions and animals would enable characterization of the systematic offset between planned and actual electrode positions, which could then be propagated as a correction factor into future planning. Finally, the absence of persistent session state in StereoPlan means that all planning parameters must be re-entered at the start of each session; implementing a session file format that saves and restores chamber geometry, insert selection, and probe placement would substantially reduce per-session setup time and the risk of transcription error between planning documents and actual drive settings.

8.5 Overall Contributions and Future Directions

This thesis makes three primary contributions to the field of systems neuroscience instrumentation. The first is a hardware contribution: two mechanically complementary multi-probe fixtures that, together, span the experimental design space between flexible multi-session cortical mapping and high-density fixed-array multimodal recording. Both designs resolve the mechanical instability that limited the two-probe predecessor, and both treat optogenetic

integration as a first-class design constraint rather than an add-on. The second is a methodological contribution: a phantom-based characterization framework for Neuropixels probe trajectories that provides empirically grounded estimates of targeting uncertainty for use in experimental planning. The third is a software contribution: StereoPlan, the first NHP-native probe trajectory planning tool to explicitly account for recording chamber geometry as the primary targeting constraint, enabling systematic pre-session planning that integrates neuroanatomical targeting, bend-tolerance analysis, and population reach computation in a single interactive interface.

Compared to the prior work reviewed in Section 2.4, the designs presented here occupy a distinct point in the design space. The Janelia multi-probe rig achieves finer independent positional control per probe but at a mechanical footprint incompatible with NHP chamber constraints. The chronic rat fixture achieves longitudinal unit stability but sacrifices session-by-session repositionability. The large-scale NHP recording system demonstrated that Neuropixels-class yields are achievable in macaques, but within a restricted cortical footprint. The present fixtures extend this capability by providing flexible, multi-area, multi-probe access across a broad cortical footprint with integrated optical stimulation support — a combination not previously available in a single platform designed from the outset for the NHP recording context.

The most important near-term future direction is in vivo validation of both fixture designs, followed by scientific experiments leveraging their complementary capabilities. The three-probe fixture is immediately suited to systematic mapping of population dynamics across PMd and M1 during skilled reaching, using the session-by-session repositionability to sample different cortical depths and locations across days while accumulating a dataset of inter-areal covariance during behavior. The six-probe fixture is suited to dense simultaneous sampling of a well-characterized

cortical region while delivering optogenetic perturbations to defined cell populations, enabling causal dissection of local circuit contributions to inter-areal signaling.

Longer-term, the modular fixture architecture and StereoPlan software platform are designed to generalize beyond the specific cortical areas targeted in this work. The chamber-agnostic design of both fixtures means they can be deployed in chambers implanted over any cortical region, and StereoPlan's grid insert system can be extended to accommodate new insert geometries by adding builder functions to the existing codebase. Together, these tools lower the barrier to multi-probe, multimodal NHP electrophysiology and provide a reusable infrastructure for the wider community studying distributed circuit dynamics in primates.

On the phantom testing side, preliminary observations suggest that 10% agarose gel may offer advantages over the ballistic gelatin used in this work for trajectory visualization. Unlike the lower-concentration agarose evaluated in Section 6.2 — which was rejected due to rapid dye diffusion and optical cloudiness — a 10% formulation has shown preliminary capability for retaining visible tracks from thin syringe insertions, likely due to the substantially higher gel density restricting lateral diffusion. Whether this track retention extends to the narrower Neuropixels shank profile (70 × 20 µm versus a syringe needle) remains to be tested. If so, 10% agarose would offer a meaningful practical advantage over ballistic gelatin: dye-stained tracks could be imaged without sectioning, enabling three-dimensional track reconstruction and potentially revealing out-of-plane curvature components that the current two-dimensional imaging approach cannot capture. Systematic comparison of 10% agarose against ballistic gelatin across a range of probe straightness profiles is therefore a recommended next step for phantom characterization work.

The six-probe fixture in its current form is a fixed-geometry assembly: once fabricated, the spatial arrangement of the six probe positions is determined and cannot be reconfigured without building a new fixture. A modular half-fixture design would substantially increase the flexibility of the system by allowing the two three-probe halves to be separated and recombined independently. This would enable experimenters to deploy three-probe subsets at adjustable inter-half separations, to mix and match halves targeting different cortical regions, and to replace a single damaged half without retiring the entire fixture. The half-fixture approach would also simplify assembly by reducing the number of probes that must be loaded and secured in a single operation, and would make dedicated assembly aids easier to design — a critical need given that the six-probe fixture currently lacks the jig support that has proven essential for the three-probe design. Developing and validating assembly aids for the six-probe fixture, whether in its current monolithic form or in a future modular half-fixture design, should be treated as a prerequisite for routine experimental use rather than an optional accessory.

Two high-priority software extensions for StereoPlan would substantially expand its practical utility. The first is support for individual subject MRI uploads. In the current implementation, all trajectory planning is performed in the space of the NMT population-average template, which introduces registration error for subjects whose brain geometry deviates from the group mean. Allowing users to load a subject-specific MRI and align it to the NMT template via manual landmark-based registration — specifying corresponding anatomical landmarks in the subject and template volumes, from which a rigid or affine transform is estimated — would enable trajectories to be planned directly in subject space. Because CHARM parcellations are already defined in NMT space, the same transform would carry atlas labels into subject space without requiring re-parcellation. This approach is implementable within the existing StereoPlan

architecture using scipy's affine transform facilities and the landmark handling already in place for the stereotaxic correction matrix.

The second high-priority extension is multi-probe planning support. The current Tab 1 workflow supports placement of a single probe at a time, with no mechanism to record and compare multiple planned trajectories simultaneously. Adding a dedicated multi-probe planning tab would allow experimenters to define, label, and adjust multiple probe entries in a single session, visualize their combined anatomical coverage in the 3D viewport and coronal panel, and export a unified planning document capturing all trajectories together. Implementation would build directly on the existing single-probe placement logic: each planned probe would be stored as an entry in a session-level list, rendered as a distinct colored actor in the viewport, and sampled independently through the existing CHARM labeling pipeline. The per-probe tissue sequences and combined footprint would then be composed into a single export, providing the kind of session-level overview that multi-probe experiments require but that the current single-probe workflow cannot produce.

Appendix

The software developed in this thesis is available at Version 1.0.0 of the repository (DOI: 10.5281/zenodo.20546040).

The hardware developed in this thesis is available at Version 1.0.0 of the repository (DOI: 10.5281/zenodo.20546336).

References

[1] J. U. Henschke and J. M. P. Pakan, “Engaging distributed cortical and cerebellar networks through motor execution, observation, and imagery,” *Front. Syst. Neurosci.*, vol. 17, p. 1165307, Apr. 2023, doi: 10.3389/fnsys.2023.1165307.

[2] S. S. Kantak, J. W. Stinear, E. R. Buch, and L. G. Cohen, “Rewiring the Brain: Potential Role of the Premotor Cortex in Motor Control, Learning, and Recovery of Function Following Brain Injury,” *Neurorehabil. Neural Repair*, vol. 26, no. 3, pp. 282–292, 2012, doi: 10.1177/1545968311420845.

[3] R. D. D’Souza and A. Burkhalter, “A Laminar Organization for Selective Cortico-Cortical Communication,” *Front. Neuroanat.*, vol. 11, p. 71, Aug. 2017, doi: 10.3389/fnana.2017.00071.

[4] J. J. Jun *et al.*, “Fully integrated silicon probes for high-density recording of neural activity,” *Nature*, vol. 551, no. 7679, pp. 232–236, Nov. 2017, doi: 10.1038/nature24636.

[5] T. Z. Luo, A. G. Bondy, D. Gupta, V. A. Elliott, C. D. Kopec, and C. D. Brody, “An approach for long-term, multi-probe Neuropixels recordings in unrestrained rats,” *eLife*, vol. 9, p. e59716, Oct. 2020, doi: 10.7554/eLife.59716.

[6] “Multi-probe Manipulation Rig,” figshare. Accessed: May 04, 2026. [Online]. Available: https://janelia.figshare.com/articles/physical_object/Multi-probe_Manipulation_Rig/31964007/1

[7] D. C. Van Essen, C. J. Donahue, T. S. Coalson, H. Kennedy, T. Hayashi, and M. F. Glasser, “Cerebral cortical folding, parcellation, and connectivity in humans, nonhuman primates, and mice,” *Proc. Natl. Acad. Sci.*, vol. 116, no. 52, pp. 26173–26180, Dec. 2019, doi: 10.1073/pnas.1902299116.

[8] J. D. Harding, “Nonhuman Primates and Translational Research: Progress, Opportunities, and Challenges,” *ILAR J.*, vol. 58, no. 2, pp. 141–150, Dec. 2017, doi: 10.1093/ilar/ilx033.

[9] P. Mahmoudi, H. Veladi, and F. G. Pakdel, “Optogenetics, Tools and Applications in Neurobiology,” *J. Med. Signals Sens.*, vol. 7, no. 2, pp. 71–79, 2017.

[10] I. H. Stevenson and K. P. Kording, “How advances in neural recording affect data analysis,” *Nat. Neurosci.*, vol. 14, no. 2, pp. 139–142, Feb. 2011, doi: 10.1038/nn.2731.

[11] A. L. Juavinett, G. Bekheet, and A. K. Churchland, “Chronically implanted Neuropixels probes enable high-yield recordings in freely moving mice,” *eLife*, vol. 8, p. e47188, doi: 10.7554/eLife.47188.

[12] “Spike sorting with Kilosort4 | Nature Methods.” Accessed: May 04, 2026. [Online]. Available: https://www.nature.com/articles/s41592-024-02232-7

[13] J. E. Chung *et al.*, “A Fully Automated Approach to Spike Sorting,” *Neuron*, vol. 95, no. 6, pp. 1381-1394.e6, Sep. 2017, doi: 10.1016/j.neuron.2017.08.030.

[14] “Drift correction — Kilosort4 0.0.1 documentation.” Accessed: May 04, 2026. [Online]. Available: https://kilosort.readthedocs.io/en/latest/drift.html

[15] R. M. McAndrew, J. L. Lingo VanGilder, S. N. Naufel, and S. I. Helms Tillery, “Individualized recording chambers for non-human primate neurophysiology,” *J. Neurosci. Methods*, vol. 207, no. 1, pp. 86–90, May 2012, doi: 10.1016/j.jneumeth.2012.03.014.

[16] C. Janson *et al.*, “Characterization of non-human primate dura in health and neurodegeneration,” Jun. 04, 2022, *bioRxiv*. doi: 10.1101/2022.06.03.477517.

[17] R. L. Spinks, S. N. Baker, A. Jackson, P. T. Khaw, and R. N. Lemon, “Problem of dural scarring in recording from awake, behaving monkeys: a solution using 5-fluorouracil,” *J. Neurophysiol.*, vol. 90, no. 2, pp. 1324–1332, Aug. 2003, doi: 10.1152/jn.00169.2003.
[18] A. Arieli, A. Grinvald, and H. Slovin, “Dural substitute for long-term imaging of cortical activity in behaving monkeys and its clinical implications,” *J. Neurosci. Methods*, vol. 114, no. 2, pp. 119–133, Mar. 2002, doi: 10.1016/s0165-0270(01)00507-6.
[19] T. Teichert, J. Grinband, J. Hirsch, and V. P. Ferrera, “Effects of heartbeat and respiration on macaque fMRI: implications for functional connectivity,” *Neuropsychologia*, vol. 48, no. 7, pp. 1886–1894, Jun. 2010, doi: 10.1016/j.neuropsychologia.2009.11.026.
[20] J. D. Power, C. J. Lynch, B. M. Silver, M. J. Dubin, A. Martin, and R. M. Jones, “Distinctions among real and apparent respiratory motions in human fMRI data,” *NeuroImage*, vol. 201, p. 116041, Nov. 2019, doi: 10.1016/j.neuroimage.2019.116041.
[21] E. M. Trautmann *et al.*, “Large-scale high-density brain-wide neural recording in nonhuman primates,” May 04, 2023, *bioRxiv*. doi: 10.1101/2023.02.01.526664.
[22] E. Zavitz and N. S. C. Price, “Understanding Sensory Information Processing Through Simultaneous Multi-area Population Recordings,” *Front. Neural Circuits*, vol. 12, p. 115, Jan. 2019, doi: 10.3389/fncir.2018.00115.
[23] E. S. Boyden, F. Zhang, E. Bamberg, G. Nagel, and K. Deisseroth, “Millisecond-timescale, genetically targeted optical control of neural activity,” *Nat. Neurosci.*, vol. 8, no. 9, pp. 1263–1268, Sep. 2005, doi: 10.1038/nn1525.
[24] A. Galvan *et al.*, “Nonhuman Primate Optogenetics: Recent Advances and Future Directions,” *J. Neurosci.*, vol. 37, no. 45, pp. 10894–10903, Nov. 2017, doi: 10.1523/JNEUROSCI.1839-17.2017.
[25] J. Hüer, P. Saxena, and S. Treue, “Pathway-selective optogenetics reveals the functional anatomy of top–down attentional modulation in the macaque visual cortex,” *Proc. Natl. Acad. Sci. U. S. A.*, vol. 121, no. 3, p. e2304511121, doi: 10.1073/pnas.2304511121.
[26] I. Ozden *et al.*, “A Coaxial Optrode As Multifunction Write-Read Probe for Optogenetic Studies in Non-Human Primates,” *J. Neurosci. Methods*, vol. 219, no. 1, pp. 142–154, Sep. 2013, doi: 10.1016/j.jneumeth.2013.06.011.
[27] “Pinpoint,” The BRAIN Initiative Alliance. Accessed: May 04, 2026. [Online]. Available: https://www.braininitiative.org/toolmakers/resources/pinpoint/
[28] “About — BrainGlobe.” Accessed: May 04, 2026. [Online]. Available: https://brainglobe.info/about.html
[29] J. E. Kleinbart *et al.*, “A Modular Implant System for Multimodal Recording and Manipulation of the Primate Brain,” in *2018 40th Annual International Conference of the IEEE Engineering in Medicine and Biology Society (EMBC)*, Jul. 2018, pp. 3362–3365. doi: 10.1109/EMBC.2018.8512993.
[30] L. I. Smith and A. L. Orsborn, “Customizable artificial simulator for developing, planning, and training personnel on neurophysiology and surgical procedures in non-human primates,” *J. Neurosci. Methods*, vol. 424, p. 110587, Dec. 2025, doi: 10.1016/j.jneumeth.2025.110587.
[31] J. Seidlitz *et al.*, “A population MRI brain template and analysis tools for the macaque,” *NeuroImage*, vol. 170, pp. 121–131, Apr. 2018, doi: 10.1016/j.neuroimage.2017.04.063.
[32] C. Reveley *et al.*, “Three-Dimensional Digital Template Atlas of the Macaque Brain,” *Cereb. Cortex*, vol. 27, no. 9, pp. 4463–4477, Sep. 2017, doi: 10.1093/cercor/bhw248.